SAE INTERNATIONAL

ARTICLE INFO
Article ID: 03-15-05-0039

doi:10.4271/03-15-05-0039

Development of a Predictive Pressure Waves Model for High-Pressure Common Rail Injection Systems

Giacomo Silvagni,[1] Vittorio Ravaglioli,[2] Fabrizio Ponti,[1] Enrico Corti,[1] Lorenzo Raggini,[1] Guido Scocozza,[1] Federico Stola,[3] and Matteo De Cesare[3]

[1]Universita degli Studi di Bologna, Italy
[2]Universita degli Studi di Bologna, Department of Industrial Engineering, Italy
[3]Marelli Europe SpA - Powertrain BU, Italy

Abstract

Over the last years, automotive industries drove a great amount of research in the field of advanced combustion techniques minimizing carbon dioxide emissions. The so-called Low-Temperature Combustions (LTC), characterized by the self-ignition of highly premixed air-fuel mixtures, represent a promising solution to achieving high efficiency and ultralow emissions of nitrogen oxides (NOx) and particulate matter. Among these, gasoline Partially Premixed Combustion (PPC), obtained through the high-pressure direct injections of gasoline, showed a good potential for the simultaneous reduction of pollutants and emissions in compression ignited engines. However, when multiple injections per cycle are performed (with hydraulic-assisted needle opening), combustion stability might be compromised by the wave effects in the hydraulic system, which produce incoherence between the requested and injected fuel. This work presents a model-based pressure waves reconstruction strategy, based on a control-oriented model of the high-pressure common rail injection system fueled with gasoline. To determine the hydraulic system's behavior during the injection process, a specifically designed flushing bench with a high-frequency acquisition system has been developed. Experimental activities have been carried out to highlight fuel pressure fluctuations with single and double injection patterns. Through the analysis of the acquired data, the key parameters (characteristic of the system) have been identified and the accuracy of pressure waves reconstruction has been evaluated, always returning errors lower than 2% between measured and estimated instantaneous pressures. Different fuel types, injectors, and rail positions have been tested to highlight the robustness of the approach. Based on the instantaneous pressure trace estimated with the control-oriented model, a fuel quantity Fluctuation Correction Strategy (FQC), implementable on a standard engine Electronic Control Unit (ECU), has been developed. The obtained results confirm the potential to reduce fuel quantity oscillations in multiple-injections systems.

History

Received: 09 Aug 2021
Revised: 12 Oct 2021
Accepted: 16 Dec 2021
e-Available: 29 Dec 2021

Keywords

Gasoline direct injection, Multiple injections, Common-rail, Pressure waves, Fuel control

Citation

Silvagni, G., Ravaglioli, V., Ponti, F., Corti, E. et al., "Development of a Predictive Pressure Waves Model for High-Pressure Common Rail Injection Systems," *SAE Int. J. Engines* 15(5):2022, doi:10.4271/03-15-05-0039.

ISSN: 1946-3936
e-ISSN: 1946-3944

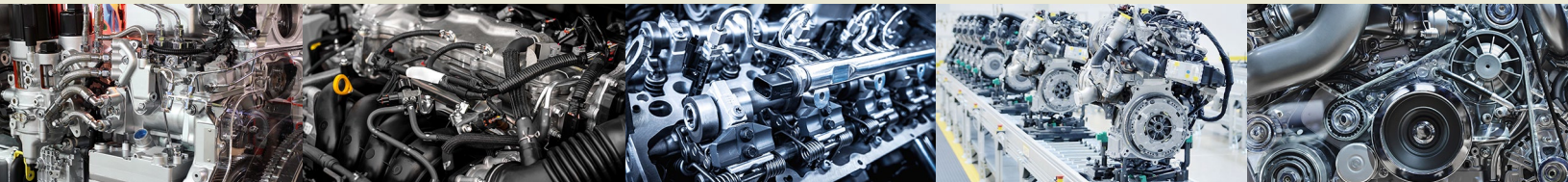

Introduction

Zero-carbon powertrains development has become one of the main challenges for automotive industries around the world. Following this guideline, powertrain electrification is considered an effective way to create a sustainable and cleaner transportation system. Many works demonstrate that purely electric-powered vehicles, such as battery electric vehicles (BEVs) and fuel cell electric vehicles (FCEVs), represent the most effective solution to achieving requirements for sustainable mobility [1, 2, 3]. However, despite enormous potential in terms of fuel-efficiency improvement, the battery-related challenges (battery cost, volume, and weight), limited autonomy, and long charging time have hindered the diffusion of BEVs. Regarding FCEVs (fueled with hydrogen) instead, despite the relatively long driving range compared to BEVs, the high cost for fuel cells, the lack (in most countries) of hydrogen filling stations and hydrogen production methods, which today mainly comes from fossil fuels, are slowing down their spread around the world. Thus, intermediate solutions in terms of electrification such as hybrid, mild-hybrid, and plug-in hybrid vehicles based on Internal Combustion Engines (ICEs) are now considered the first step moving toward transportation 2.0 [3]. For these reasons, ICE development is still crucial to produce more and more efficient and cleaner hybrid powertrains (electric + ICE), overcoming the well-known limitations of full-electric vehicles (BEVs and FCEVs) [2, 3].

With the aim of improving both combustion efficiency and engine-out emissions, over the past years, the research community has investigated innovative combustion approaches called Low-Temperature Combustions (LTC) [4, 5, 6, 7], which have shown good potential in achieving both goals. Based on the combustion of lean air-fuel mixtures under unthrottled conditions and high compression ratios, those techniques have shown Brake-Specific Fuel Consumption (BSFC) lower than 200 g/kWh, with ultralow emissions of nitrogen oxides (NOx) and particulate matter (PM) [5, 6].

Homogeneous-Charge Compression Ignition (HCCI) is the most studied LTC approach, characterized by compression ignition of fully homogeneous air-fuel mixture [4, 7, 8, 9, 10]. A great amount of research has been made by Dempsey et al. [7], Li et al. [10], Dernotte et al. [11], and Kolodziej et al. [12] on HCCI, reporting big advantages in efficiency and emissions compared to other conventional combustions. Besides, they have also highlighted HCCI's high knock tendency and low controllability as a result of its ignition mechanism, mainly driven by chemical kinetics and thermodynamic conditions [8, 9, 13].

A potential solution to overcome HCCI applicability limits is gasoline Partially Premixed Combustion (PPC), which combines the high efficiency of compression ignition engines, due to high compression ratio and unthrottled operation, with the advantageous gasoline-like fuel properties, such as high resistance to autoignition as well as high volatility. As widely reported in the literature [14, 15, 16, 17], to properly control gasoline PPC combustion, a high-pressure multiple direct injection strategy is needed. As a matter of fact, previous works [18, 19] clearly show the enormous benefit given by pilot injections both in terms of pollutants reduction, such as NOx, and combustion stability improvements. As for Conventional Diesel Combustion (CDC), the rise of in-cylinder pressure and temperature generated by pilot injections combustion allows minimizing the ignition delay of the following injections, making the whole combustion process more stable and smoother. As a result, proper management of pilot injections in terms of injected fuel quantity, number of injections, and angular positions plays a key role to ensure gasoline PPC controllability, especially the center of combustion and delivered torque [20, 21].

To meet such requirements, the high-pressure Common Rail (CR) system represents the most common injection system testing gasoline PPC [19, 20, 22]. Thanks to the use of solenoid hydraulic assisted injectors, modern CR systems guarantee fast and accurate injection management also with the high pressures required by gasoline PPC (up to 1000 bar) [22, 23, 24, 25]. Despite the high flexibility performing multiple injections with CR systems, hydrodynamic effects, which are generated by the water hammer consequent to the injector nozzle closing after each injection, affect the actual quantity of fuel injected during the following injections [26, 27, 28, 29, 30, 31, 32], especially when the amount of fuel injected is very low (in the range of 1 mg/str) and the relative distance between injections is small (lower than 2000 μs). As widely discussed in the literature [33, 34, 35, 36, 37, 38, 39, 40, 41, 42, 43], due to the propagation of pressure waves, the mass of fuel injected during the second of two consecutive injection pulses may vary significantly (up to 50%) around the nominal value, producing negative effects on the gasoline PPC stability [25, 37]. Thus a fuel quantity correction strategy is required to achieve accurate fuel injection management.

With the aim of investigating pressure waves and their effects on the injection quantity, several approaches have been used. Coppo et al. [26] presented a numerical model for a CR system finding that the hydraulic layout (feed duct length and diameter) and injector nozzle had a relevant impact on pressure wave propagation. Boudy et al. [28] investigated the influence of fuel properties on the pressure wave in the injector feed duct. They found that fuel density is the main property that influences the amount of mass injected because it changes fuel viscosity and bulk modulus. Based on the abovementioned findings, many works have been focused on clearing pressure waves effects. Su et al. [39] experimentally obtained an ideal filter for the elimination of the water hammer. Gupta et al. [40], Bianchi et al. [31, 41], and Ferrari et al. [32, 35, 38] showed that water hammer effects can be reduced by changing the system layout but increasing the cost of designing and manufacturing of the whole injection system. Bai et al. [37] presented a correction strategy based on the reconstruction of injected quantity oscillations, for a typical pilot-main injection strategy, without taking into account the source of this phenomenon, i.e., pressure waves.

In this work, a physical model of pressure waves propagating in a standard high-pressure CR system fueled with

gasoline based on the equivalent mass-spring-damper (MSD) system is presented. Through a specifically designed flushing bench equipped with a high-frequency acquisition system, a wide experimental activity has been conducted highlighting pressure waves behavior on the feed duct using different injection strategies. To properly reconstruct pressure waves propagation on the feed duct, a frequency analysis, aimed at finding the main carriers of the pressure waves (both with single and multiple injections), has been carried out varying fuel injection pressure and Dwell Time (DT) between injections. To verify the model applicability and robustness, different fuel, injector, and placement on the rail have been tested. Finally, the obtained results were used to develop a fuel quantity Fluctuation Correction Strategy (FQC) based on the pressure wave reconstruction during multiple injections of gasoline.

Experimental Setup

The experimental activity was carried out on a specifically designed high-pressure CR test bench, based on a light-duty 1.3L diesel engine injection system with four solenoid injectors fueled with RON 95 commercial gasoline. In order to study pressure waves under actual operating conditions, the high-pressure line has not been changed with respect to the engine-mounted configuration, i.e., pipeline diameter and length have been maintained as in the original layout. The main technical characteristics of the CR system under study are summarized in Table 1.

To simulate the fuel thermal inertia on CR low-pressure side (which is typically composed of long pipes connecting the tank with the high-pressure pump), a diathermic oil thermoregulation unit (TEMPCO T-REG HCE 609/15-O) has been installed between the low-pressure pump and the high-pressure pump. The thermoregulation unit allowed to accurately manage the fuel temperature during all tested conditions excluding external thermal effects on the pressure wave propagation, such as frequency or amplitude modifications [20, 29]. Furthermore, to consider the fuel tank thermal inertia, a water-fuel heat exchanger has been placed before the low-pressure pump. Finally, the low-pressure line was kept at a constant pressure of 4.5 barA (standard condition for the CR system under study) using a mechanical pressure regulator.

TABLE 1 High-pressure CR system technical characteristics.

Number of injectors	4
CR pump	Bosch CP1
Injector type	CRI2-16 M2
Feed duct length	93 mm
Feed duct diameter	20 mm
External rail length	250 mm
External rail diameter	200 mm

To accurately investigate pressure waves and their consequences on the effectively injected fuel, several sensors have been mounted on the test bench. In addition to standard CR system sensors, i.e., rail-mounted high-pressure fuel sensor (PRail) and low-pressure and temperature fuel sensors, to highlight pressure wave behavior during the injection process, the high-pressure pipe between the rail and the injector has been equipped with two piezoresistive pressure sensors Kistler 4067A, one close to the injector (PKist Inj Side) and the other close to the rail (PKist Rail Side). Furthermore, to monitor the oscillations in injected fuel generated by water hammer propagation, two different gasoline consumption measurement systems (AVL Balance 733S and high-precision ultrasonic flowmeter FlowSonic FFM LF DP-010-02) have been installed on the test bench low-pressure line. Both measurement systems are fully closed (AVL Balance closed vessel and FFM closed pipe) to avoid fuel evaporation and, consequently, exclude measurement errors when high volatile fuels are used. Fuel consumption measurement redundancy allowed the authors to define proper acquisition strategies for each tested injection pattern, obtaining consistent consumption measurements also with different instruments and small injected quantities. These strategies provided a reliable fuel consumption measurement also when a different fuel was used (the high-precision ultrasonic fuel consumption measurement was not available for both tested fuels). Finally, with the purpose of monitoring the heat exchange between fuel and diathermic oil (on the fuel side), two K-type thermocouples between the inlet and outlet of the TEMPCO heat exchanger were mounted. Figure 1 shows the hydraulic layout of the high-pressure test bench.

Test bench control and data acquisition have been managed by a specifically developed Rapid Control Prototyping (RCP) system based on National Instruments cRIO 9082 using LabView. Selecting proper acquisition frequencies for each signal (100 kHz for high-pressure sensors, to keep all the main carriers of the injection system significantly lower than the Nyquist frequency), the RCP system allowed to collect all the data needed for pressure waves analysis and modeling.

Regarding the fuel pressure management, it was performed to keep in motion the volumetric high-pressure pump with an electric motor (5.5 kW and maximum rotational speed of 3000 rpm) at constant revolutions per minute (rpm). The mechanical connection between the high-pressure pump and the electric motor, obtained with a toothed belt, was designed with the same gear ratio used in the onboard application for the connection between the crankshaft and pump (the electric motor rotates twice as fast as the pump). Using the information coming from the encoder mounted on the pump shaft, the RCP system evaluated the pump speed, sending an analog command to a dedicated inverter managing the electric motor. Furthermore, acquiring the rail-mounted pressure sensor, the RCP system was able to manage the Pulse Width Modulation (PWM) command of the pump-mounted

FIGURE 1 Flushing bench hydraulic layout.

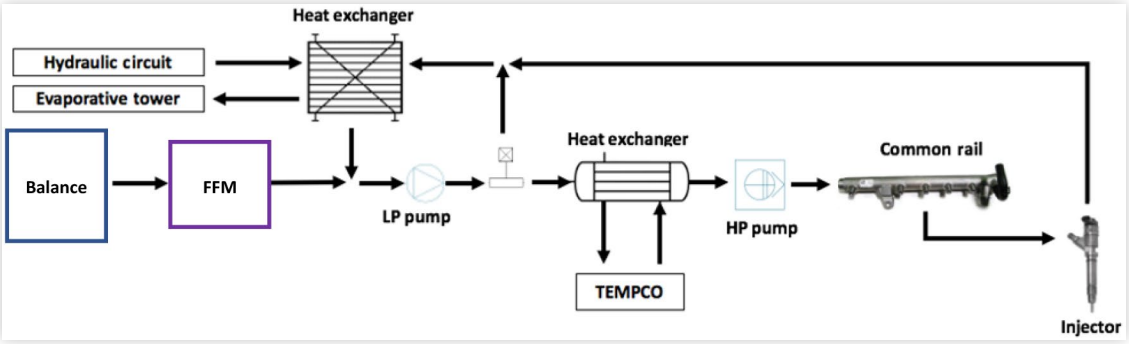

solenoid metering valve (MPROP) to keep the fuel pressure at the target value during each test. A picture of the high-pressure CR test bench is shown in Figure 2.

The injection strategy has been managed using a fully programmable Electronic Control Unit (ECU) (SPARK by Alma Automotive), based on National Instruments hardware and LabView software, overcoming the limitations that usually occur when a production ECU with standard control software is used with custom injection patterns. Despite the fact that the MPROP valve can be easily managed by SPARK ECU, with the aim of improving the test bench safety during the experimental activity, both MPROP duty and pump speed have been managed by the RCP system. Furthermore, to improve testing operations, the injection parameters were controlled and logged using INCA software, provided by ETAS. Figure 3 reports the test bench control layout and the integration between the RCP system and SPARK ECU.

Pressure Waves Physical Model

The above-described testing layout, specifically realized for this work, was used to investigate pressure waves under different injection strategies, the goal being to develop a model-based pressure waves reconstruction (and compensation) strategy.

Hydraulic System Behavior Analysis

In literature, several works can be found [25, 27, 29, 34, 36] describing the CR system behavior from different points of view: equivalent electrical, rotational, thermal, chemical, and mechanical systems have been proposed. Furthermore, they

FIGURE 2 Flushing bench pressure sensors placement.

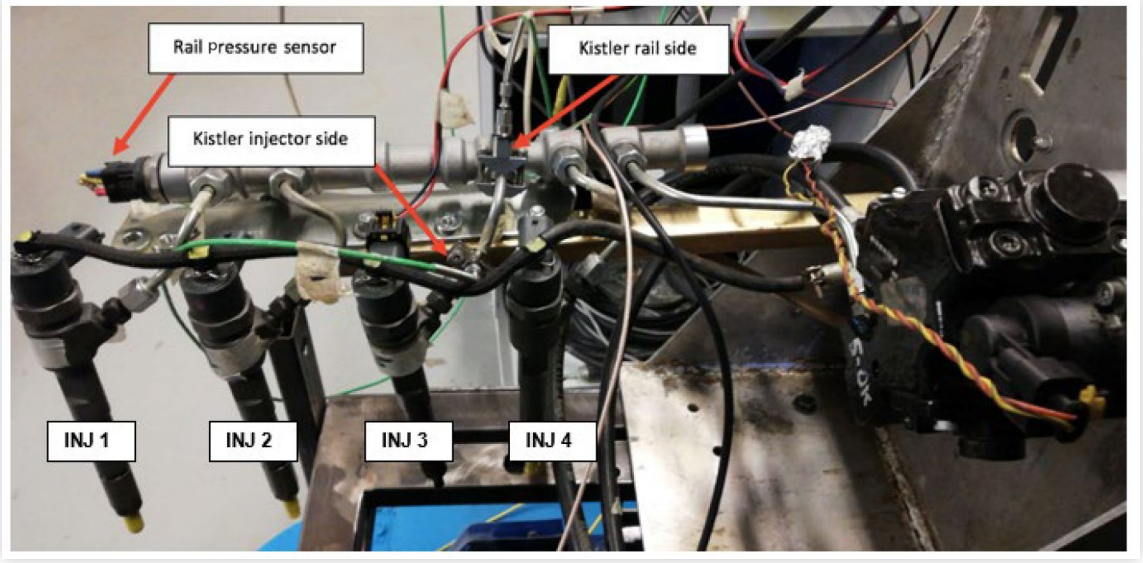

FIGURE 3 Scheme of flushing bench control and acquisition systems.

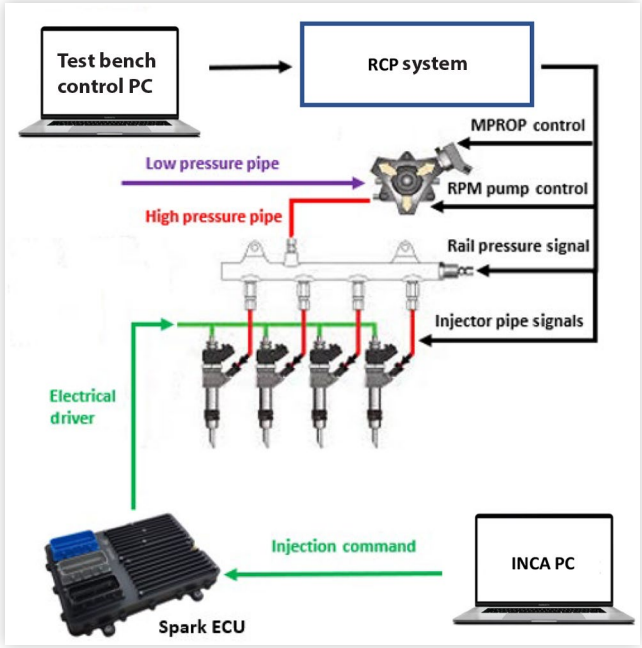

Laptop images: Shutterstock.com/ BGStock72

also report that it is possible to obtain transfer functions linking the physical CR system properties with the equivalent system characteristics parameters [40, 41, 42, 43]. Therefore, with the aim of identifying the best approach to model pressure waves in the CR system, the authors focused the first part of the experimental activity on the study of the system behavior performing gasoline single injections. To do so, the whole experimental activity has been carried out keeping three injectors closed (but connected to the rail) and activating only one injector.

Figure 4 shows the pressure signals coming from rail-mounted and high-pressure tubing-mounted sensors for a single injection pulse test and injection pressure of 700 bar. By the analysis of the piezoresistive pressure sensors signals, it is possible to notice that, when the injection occurs, a high-frequency pressure wave is generated. This wave, produced by the mass discharged from the injector, propagates inside the feed duct from the injection event up to 20 ms after, when its energy is totally dissipated [42, 43]. Because of the larger amount of fuel contained in the rail compared to that in the feed duct, and due to the pressure drop generated by the duct-to-rail connection, the rail capacity can be considered as infinite, and therefore, the rail-mounted pressure signal (PRail) does not contain the information of pressure oscillations. This evidence, confirmed by the literature, suggests that the pressure wave triggered by the injection propagates only inside each feed duct without generating cumulative effects in the near ducts.

In addition, it is clear from the comparison of the piezoresistive sensors' pressure traces that the effects of pressure waves are more visible, in terms of oscillations amplitude, closer to the injector. For this reason, to model the pressure oscillations generated by single and multiple injections, the authors will consider the pressure traces coming from the piezoresistive pressure sensor closer to the injector because they represent the instantaneous fuel pressure, which directly determines the injected mass.

Furthermore, it is important to notice that both duct and rail-mounted sensors show a low-frequency oscillation representing the leakage flow rate compensation due to the closed-loop rail pressure controller behavior. As clearly highlighted by Figure 5(a), the instantaneous pressure traces acquired by

FIGURE 4 Experimental fuel pressure signals (acquired at 100 kHz) generated by a single injection (per cycle, only one injector active) pulse strategy at gasoline pressure 700 bar, 1000 pump rpm, and ET of 310 μs.

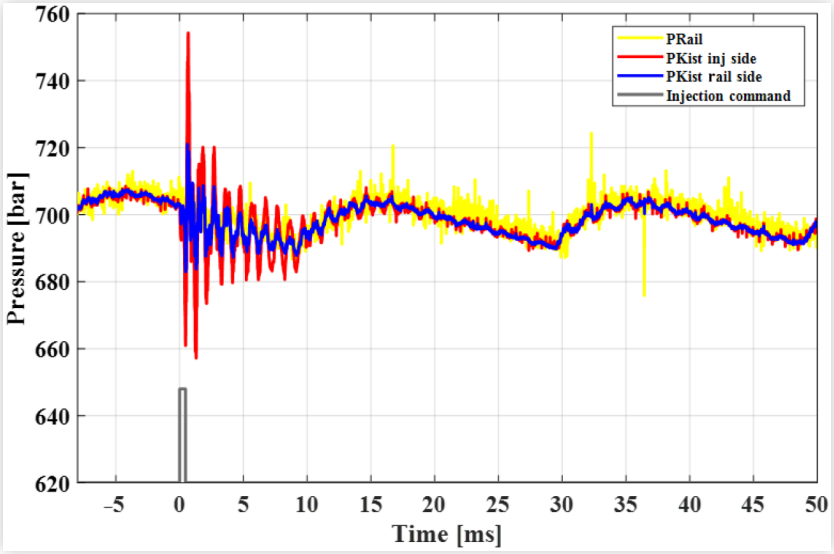

FIGURE 5 Piezoresistive injector-side pressure signals for (a) different injection cycles (acquired at 100 kHz) and (b) the average of 500 consecutive injection cycles at gasoline pressure 700 bar, 1000 pump rpm, and ET of 310 μs.

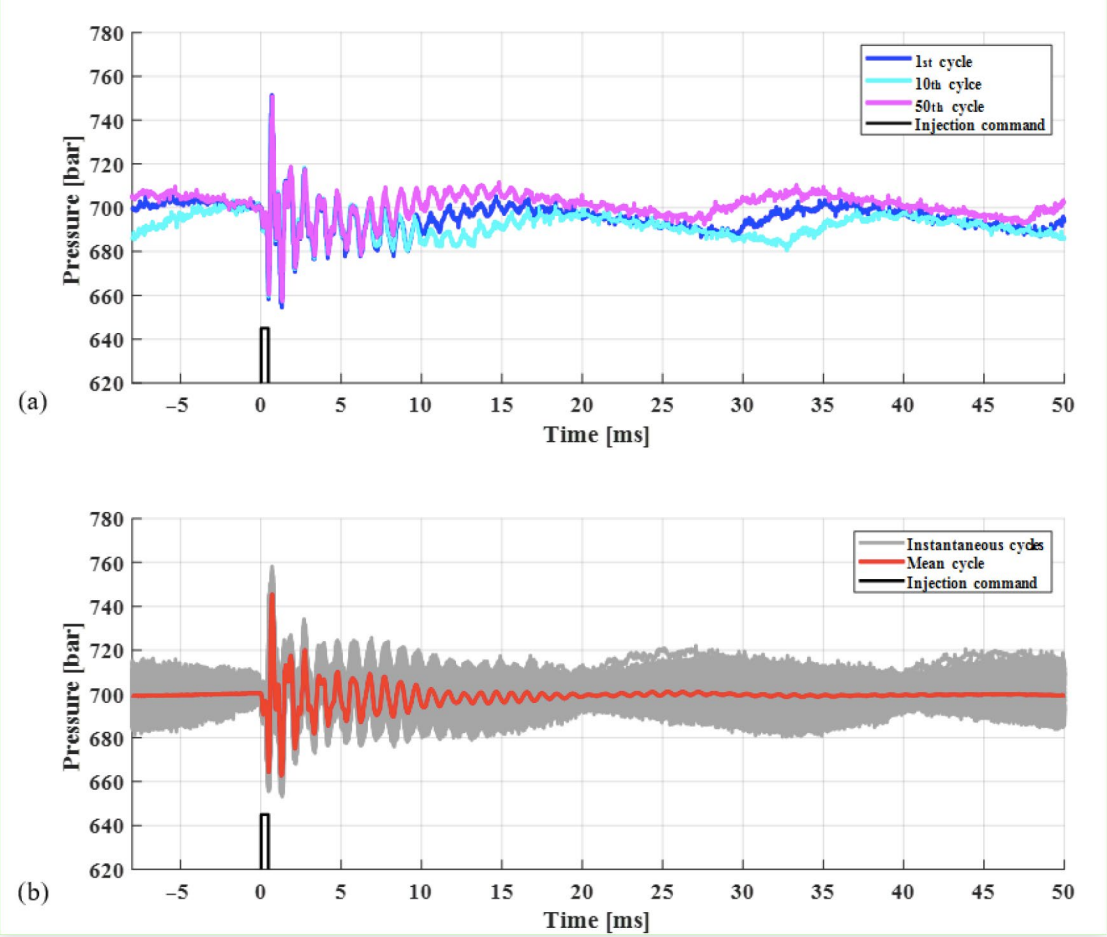

the sensor closer to the injector during different injection cycles show the same high-frequency oscillations generated by the injection, but different low-frequency oscillations. The position of the leakage flow rate contribution moves on the injection cycle because the pressure controller actuation, which manages the MPROP valve duty cycle keeping constant rail pressure, is not phased with the injection event shifting the leakage compensation with respect to the injection pulse.

To highlight the portion of the pressure oscillations related to the injection process, the average of 500 consecutive injection cycles has been considered. As Figure 5(b) clearly shows, averaging the pressure traces mitigated the acquisition noise and the leakage flow rate effect, highlighting only the pressure wave of interest (which occurs cycle by cycle) and its propagation time (from the injection event to 20 ms). Moreover, it is possible to see that the leakage contribution does not affect the bulk of the pressure oscillation (from 0 to 10 ms), but it becomes predominant when the oscillation amplitude decreases (10 ms after the injection event). For these reasons, the hydraulic system modeling was based on the average pressure trace reconstruction. As a result, the fuel system's external conditions such as pump speed (even during transients) or the MPROP duty cycle, which change only the leakage contribution, do not affect the modeling.

From the observation of Figure 5(b), it arises that the average pressure trace during the injection cycle follows the typical behavior of an underdamped MSD vibration system. For this reason, in order to accurately predict the pressure wave in the feed duct triggered by the injection, a mechanical approach has been followed. Finally, it is important to underline before the prominent pressure oscillations the effect of the injector opening dynamics in terms of pressure drop. The upcoming section describes the pressure wave modeling approach based on the MSD system.

Hydraulic System Modeling

In agreement with the similarity principle between mechanical and hydraulic systems [36, 43], this work assumes the pressure wave during the injection process as the sum of free responses of one-degree-of-freedom MSD systems, one for each main carrier contained in the experimental signal.

FIGURE 6 Schematic of an MSD one-degree-of-freedom system.

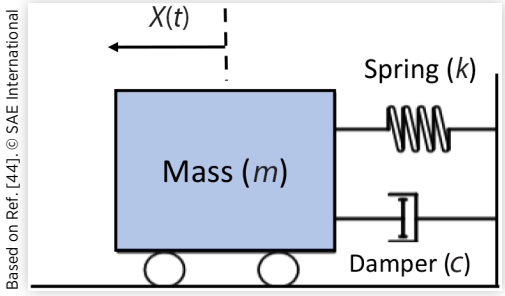

The free-response calculation for the well-known one-degree-of-freedom MSD system can be based on the analysis of the system reported in Figure 6 [44].

Equation 1 describes the motion of the system, in which x is the pressure on the feed duct. The system parameters m, k, and c represent the fuel inertia of the feed duct and injector, the fuel stiffness, and the damping, respectively.

$$m\ddot{x} + c\dot{x} + kx = 0 \qquad \text{Eq. (1)}$$

Considering as solution of Equation 1 the typical exponential form shown in Equation 2 [44], the characteristic equation of the vibration system can be obtained. As reported in Equation 3, it is a linear, ordinary homogeneous differential equation with constant coefficients.

$$x(t) = Ce^{zt} \qquad \text{Eq. (2)}$$

$$mz^2 + cz + k = 0 \qquad \text{Eq. (3)}$$

Thus the natural frequency of the vibrational system ω_n and the damping ratio ξ can be defined as reported in Equations 4 and 5, respectively.

$$\omega_n = \sqrt{\frac{k}{m}} \qquad \text{Eq. (4)}$$

$$\xi = \frac{c}{2\sqrt{km}} \qquad \text{Eq. (5)}$$

For the analysis of the damped system, it is useful to define the damped frequency of the vibrational system ω_d as a function of ω_n and ξ (Equation 6), which represents the actual frequency of the oscillation.

$$\omega_d = \omega_n \sqrt{1-\xi^2} \qquad \text{Eq. (6)}$$

Solving the differential equation shown in Equation 2 and applying the well-known Euler's formula, the free response of the MSD system can be written as reported in Equation 7, where, in addition to the above-mentioned parameters, x_0 and v_0 have been considered as initial conditions (time equal to zero) of the system.

$$x(t) = e^{-\xi\omega_n t}\left(x_0\cos(\omega_d t) + \frac{v_0 + \xi\omega_n x_0}{\omega_d}\sin(\omega_d t)\right) \qquad \text{Eq. (7)}$$

The following section describes the methodology developed by the authors to reconstruct the pressure oscillations during the injection cycle, based on a sum of one-degree-of-freedom MSD systems free responses, Equation 7.

Hydraulic System Characterization

In order to identify the number of free responses needed to reconstruct the pressure oscillations and highlight the main injection parameters effects on the hydraulic system behavior, such as injection duration (ET) and injection pressure, a frequency analysis for a single pulse injection strategy has been performed.

The frequency content of the pressure oscillations can be summarized in Figure 7, which reports the pressure signal power spectrum from 0 to 4 kHz (higher frequencies do not have relevant energy content) for a single pulse injection strategy with a gasoline pressure of 500 bar using different ETs. It is important to notice that changing the injection duration, i.e., increasing ET, the power spectrum changes in amplitude but not in frequency. It means that the injection duration affects only the amplitude of the response without any modification in terms of frequency content.

The power spectrum, Figure 7, also shows five main carriers: the first around 16.6 Hz related to the injection frequency, the second at 600 Hz, the third at 830 Hz, the fourth at 1.05 kHz, and the fifth at 2.2 kHz related to the system behavior (rail, duct, and injector). Considering the identified main carriers, it is possible to notice that the first frequency can be neglected because it is not related to the pressure oscillation but only to the injection cycle (the frequency of 16.6 Hz corresponds to 1000 pump rpm, or 2000 engine rpm). The third frequency can be considered the fundamental frequency of the hydraulic system because it shows the biggest amplitude for all the tested conditions. Due to the small distance in frequency and the huge difference in amplitude of the second and the fourth main carriers with respect to the fundamental frequency, their contribution to the pressure fluctuation is not clearly visible in the instantaneous pressure trace. This observation suggests that the second and the fourth frequencies could be neglected while modeling the pressure wave. On the contrary, despite the smaller amplitude of the fifth component (compared to the fundamental), the higher frequency makes it clearly visible in the pressure oscillation.

Based on the above-described considerations, to quantify the relevance on the pressure oscillation of each main carrier with respect to the fundamental frequency, the Relevance Carrier Index (RCI) has been defined as reported in Equation 8. This index is composed of the product between the relative power ratio (P_{r_x}), which represent the energy contribution of

FIGURE 7 Frequency analysis (power spectrum) of the injector-side pressure signal generated by single injection pulse strategy at different ETs with gasoline pressure 700 bar and 1000 pump rpm.

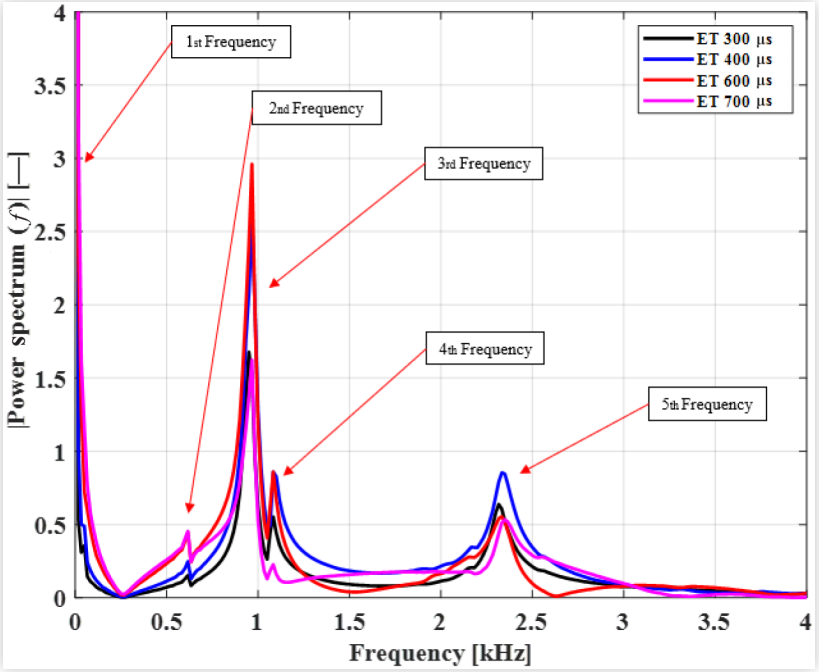

the specific x-th carrier compared to the total energy of the identified main carriers ($\sum_i P_i$), and the frequency distance (ΔF_x) from the third frequency. Equations 9 and 10 define the relative power ratio and the frequency distance, respectively.

$$\mathrm{RCI} = P_{r\_x}\Delta F_x \qquad \text{Eq. (8)}$$

$$P_{r\_x} = \frac{P_x}{\sum_i P_i} \qquad \text{Eq. (9)}$$

$$\Delta F_x = \frac{F_x - F_3}{F_3} \qquad \text{Eq. (10)}$$

Table 2 reports the RCI calculation for the power spectrum shown in Figure 7 at ET = 400 µs. As it can be seen, despite the amplitude of the fourth and fifth carriers being similar, the huge differences in the calculated RCI suggest that the fifth frequency cannot be neglected to properly reconstruct the pressure oscillation. On the contrary, it is reasonable to expect that the second and fourth frequency might be neglected without losses of information in the reconstruction of the pressure fluctuation. This assumption will be further discussed and confirmed, through the analysis of the experimental acquisitions, in the following section.

TABLE 2 RCI estimation at ET = 400 µs with gasoline pressure 700 bar and 1000 pump rpm.

Carrier number	Frequency [Hz]	Amplitude [—]	Relative frequency [%]	RCI [—]
2nd	616	0.247	35.8	1.94
3rd	960	2.596	—	—
4th	1083 700	0.858	12.8	2.41
5th	2330	0.853	142.7	26.73

According to the considerations based on the power spectrum, the pressure wave during the injection process can be modeled as a sum of two one-degree-of-freedom MSD systems free responses, representing the third and fifth main carriers (which are the larger part of raw signal energy content).

As widely reported in the literature [25, 26, 30], the injection pressure does not modify the hydraulic system characteristics but only the fuel stiffness. Figure 8 clearly shows that in changing the fuel pressure (keeping the injected mass constant at 1 mg/str) the power spectrum will maintain its typical shape, but with different frequencies. Indeed in increasing the fuel pressure, all carriers move to higher frequencies, keeping constant their relative position. Furthermore, it can also be seen that for all the tested injection pressures, the larger part of the energy content of the signal is represented by the third and fifth main carriers. Once again, the considerations based on the power spectrum confirm that the pressure wave during a single pulse injection strategy can be modeled as the sum of the responses of two one-degree-of-freedom MSD vibration systems.

As shown in Equation 7, the one-degree-of-freedom MSD vibration system free response is a function of the system parameters, i.e., ω_d, ξ, x_0, and v_0. With the aim of obtaining the abovementioned parameters for both the main carriers (the third and the fifth), a numerical optimization for the

FIGURE 8 Frequency analysis (power spectrum) of the injector-side pressure signal generated by single injection pulse strategy at different gasoline pressures with the same injected mass (1 mg/str) and 1000 pump rpm.

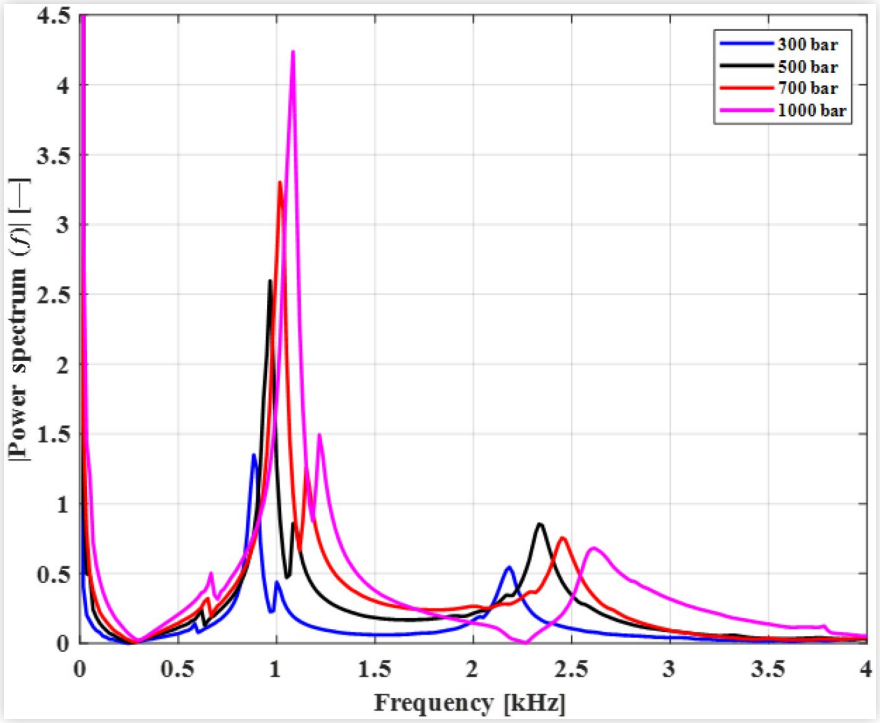

single pulse injection strategy has been performed. Starting from the general formulation of the free response shown in Equation 7, the optimization process, based on MATLAB *fminsearch* function, calculates the four fundamental parameters (ω_n, ξ, x_0, and v_0) minimizing the distance between the mathematical model and a bandpass filtered pressure signal centered on the analyzed frequency. The optimization process has been applied for both the main carriers at all tested conditions in terms of ET and gasoline pressure. Figures 9 and 10 summarize the output of the optimization process (eight fundamental parameters) as a function of ET and gasoline pressure.

Analyzing the obtained maps, Figures 9 and 10, it is important to highlight that all the parameters show clear dependencies with respect to gasoline pressure and ET except ξ_1, ω_{n1}, and ω_{n2}. As mentioned previously, the injection duration does not modify the hydraulic system behavior; hence, the frequencies (ω_{n1} and ω_{n2}) can be considered constant for different ETs and linearly variable with respect to the injection pressure (increasing the rail pressure both frequencies will rise).

Regarding ξ_1, the optimization provides as output very close values for each tested condition, and a defined trend cannot be determined. This means that ξ_1 is unsensitive with respect to the injection parameters. Consequently, an average (constant) value of ξ_1 can be reasonably chosen to replace the reported map. As clearly visible in Figure 10(b), the situation is slightly different for the fifth main carrier because the damping ratio ξ_2 tends to increase with the rail pressure (for a fixed ET) and decrease with higher values of ET (for a given rail pressure).

Figure 7 shows that the complete power spectrum contains many frequencies with lower energy content with respect to the identified main carriers. Since the total energy content of the other frequencies is not negligible, considering only the sum of the modeled main carriers would lead to an inaccurate reconstruction of the instantaneous pressure trace. To take into consideration the total energy contribution from frequencies different from the two main carriers, the estimated pressure fluctuation has been corrected using a set of specifically identified offsets and gains, mapped as functions of rail pressure and energizing time. The last step of the system characterization was to obtain the maps of gain and offset applied to the reconstructed pressure oscillation, which allows compensating the energy content lost by considering a simplified power spectrum (with only two main carriers). The offsets have been determined as the difference between the mean values of the modeled and experimental pressure oscillation, while the gains have been calculated as the ratio between the first absolute peaks of the modeled and experimental pressure oscillation. Figure 11 reports the obtained maps. It is interesting to notice that the offset map shows a clear dependence on both ET and rail pressure, while the gain map shows a slight correlation with respect to ET and no evident dependence on the rail pressure.

FIGURE 9 MSD system parameters after the optimization process for the first main carrier as a function of injection parameters (injection pressure and ET): (a) frequency ω_d, (b) damping ξ, and initial conditions (c) and (d) for x_0 and v_0, respectively.

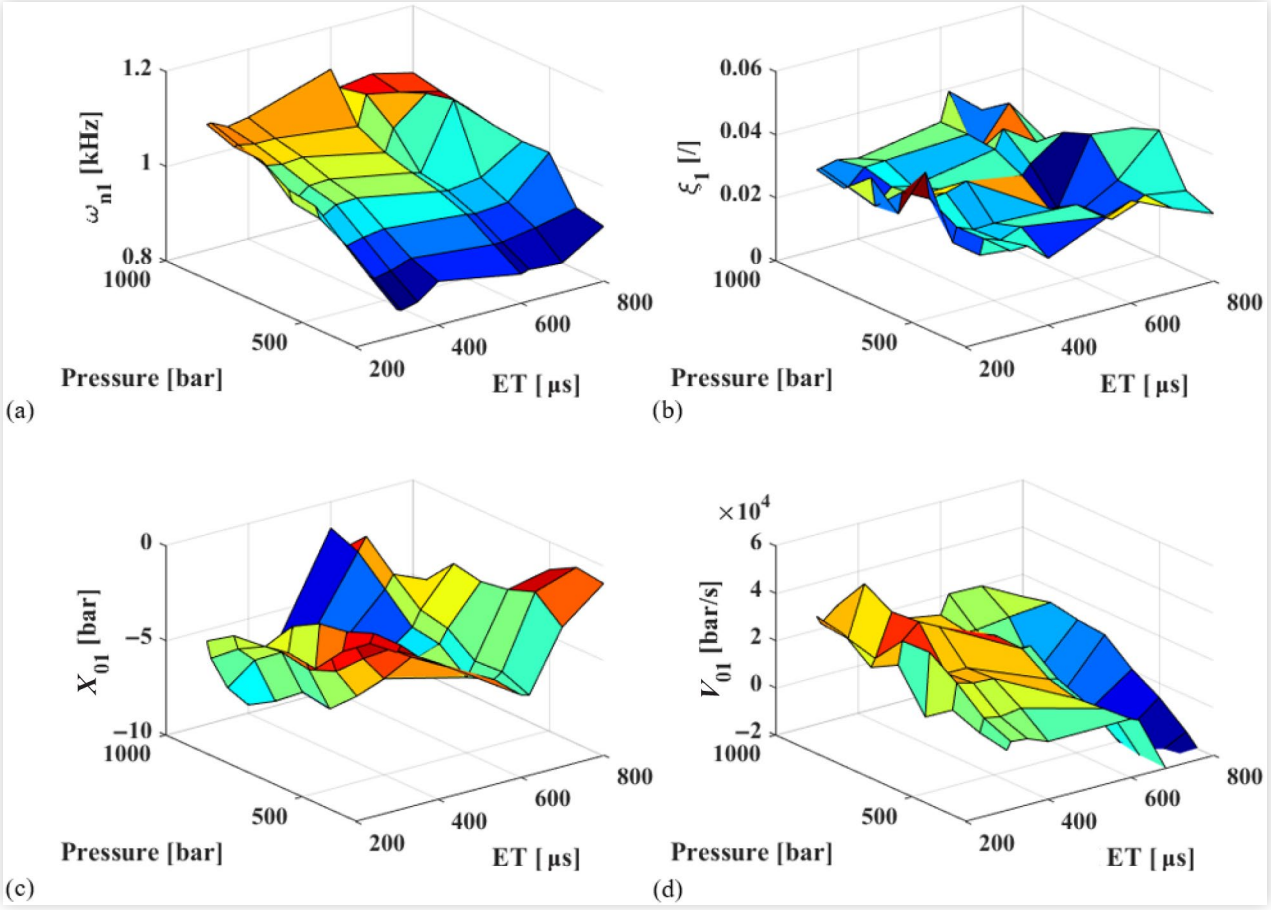

Results and Discussion

After obtaining the hydraulic system characteristics as described in the previous section, the pressure waves reconstructions were derived applying the model-based approach under different injection strategies (single and multiple injections) and conditions, such as injection pressure, ET, and relative position between consecutive injections. Since the aim of the modeling approach is to develop a control strategy suitable to mitigate the fuel quantity oscillation during multiple injections of gasoline, typical values of the injection parameters used for the management of gasoline PPC were tested. As a result, the single injection strategy was tested varying the rail pressure from 300 bar to 1000 bar and the injected mass from 1 mg/str to 45 mg/str (for the highest pressure). Once the pressure waves reconstruction was validated for the single injection strategy, with the aim of verifying the model-based approach applicability also with multiple injections, an experimental activity was carried out performing two consecutive injections with the same ET and different DTs (defined in Equation 11).

$$DT = \frac{(EOI_1 - SOI_2) \times RPM}{10^6} \qquad \text{Eq. (11)}$$

Table 3 summarizes all tested conditions using gasoline, the goal being to validate the pressure wave reconstruction by comparing them with the experimental pressure trace. It is important to underline that the whole experimental activity has been carried out keeping the injector nozzle at the atmospheric pressure (without backpressure). As well known, the backpressure on the nozzle changes the total injected mass (i.e., the injector map which is calibrated with the typical in-cylinder pressure on the nozzle) but does not affect the hydraulic system behavior (especially its characteristic frequencies). As a result, the pressure waves estimation methodology can be considered valid also when the backpressure is varied.

FIGURE 10 MSD system parameters after the optimization process for the second main carrier as a function of injection parameters (injection pressure and ET): (a) frequency ω_n, (b) damping ξ, and initial conditions (c) and (d) for x_0 and v_0, respectively.

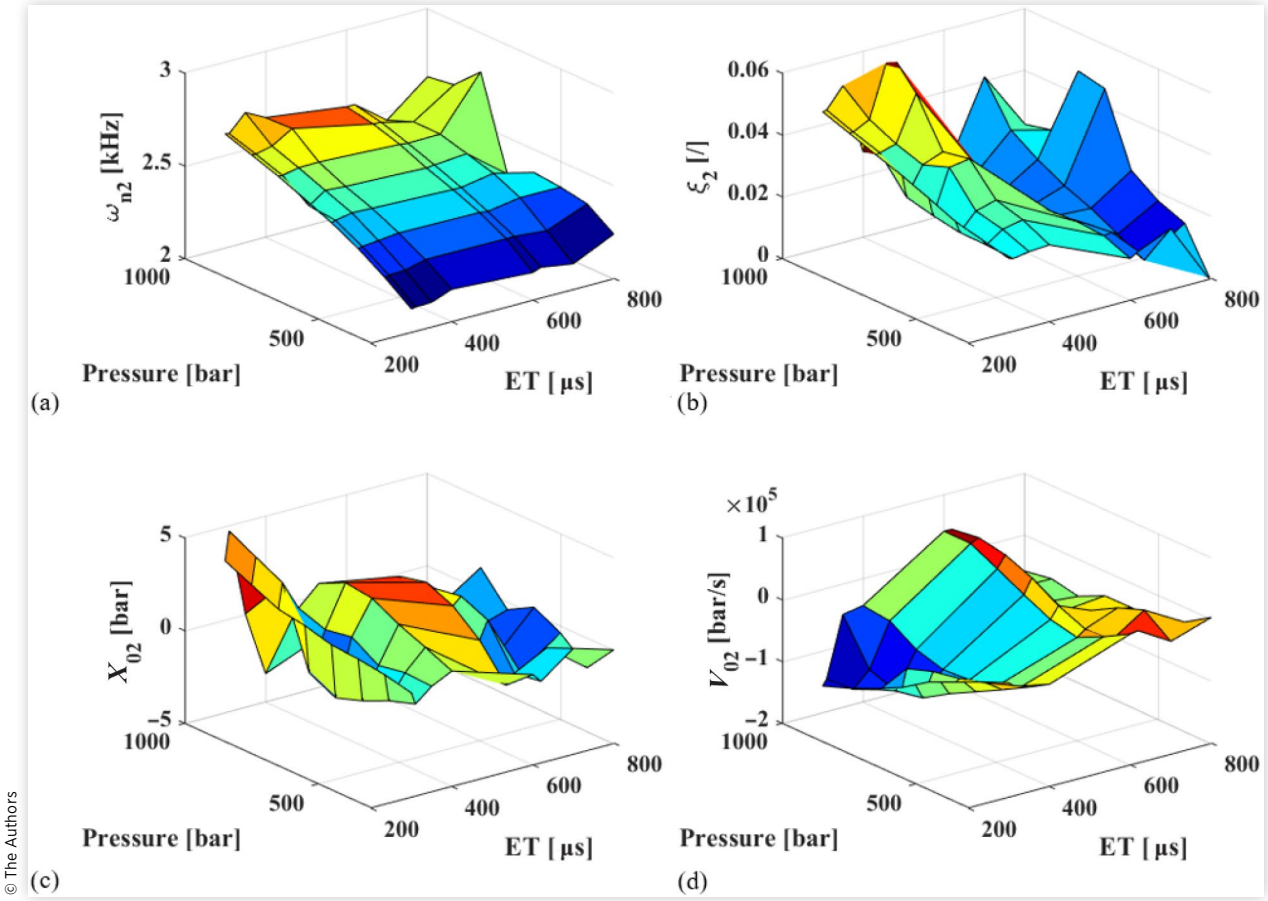

FIGURE 11 Gain (a) and offset (b) maps for the reconstructed pressure trace.

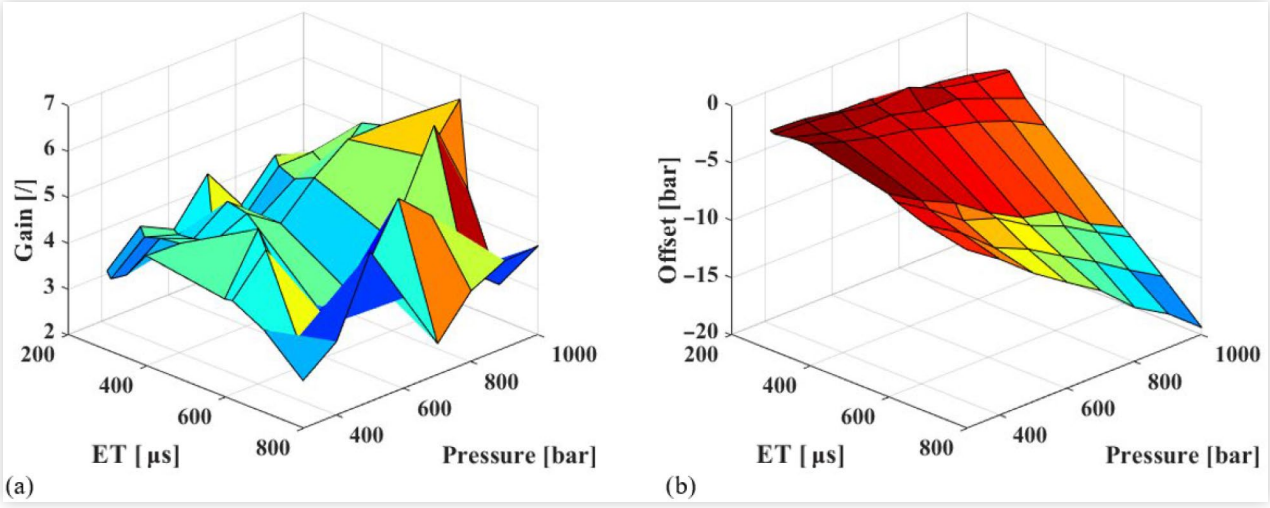

TABLE 3 Test plan of the experimental activity.

Injection strategy	PRail [bar]	ET 1 [μs]	ET 2 [μs]	DT [μs]
Single	300 to 1000	300 to 800	—	—
Double	300	400	400	20 to 3800
Double	500	350	350	20 to 3800
Double	700	310	310	20 to 3800
Double	1000	300	300	20 to 3800

Pressure Wave Reconstruction for Single Injection Strategy

First, the goal was to verify the model-based approach robustness reproducing the pressure wave generated by a single injection pulse using the hydraulic system parameters obtained by the optimization process. Following the control scheme reported in Figure 12, the pressure waves were simulated as the sum of two MSD free responses, one for each identified main carrier (third and fifth frequencies). The MSD system parameters were obtained using the above-described maps considering the ET and injection pressure (PRail) as input variables. Finally, by using the offset and gain maps (ET and PRail as inputs), the pressure wave reconstruction strategy for single injection (SI-PWR) retrieves the energy content of the neglected frequencies (mainly the second and fourth frequencies).

Figure 13 shows the comparison between simulated and experimental pressure waves considering only the oscillation contribution for different ET at a gasoline pressure of 700 bar. It is important to underline that the developed model-based approach does not consider the injector dynamics [31]; therefore, the pressure drop generated by the injector opening has been neglected. The pressure waves simulations start from the first pressure drop generated by the mass discharged from the injector. To estimate the simulations' accuracy during the propagation phase of the waves, the percentage error has been defined as reported in Equation 12. The percentage error definition allows comparing the pressure wave reconstruction accuracy for different injection pressure settings.

$$\text{Error } \% = \frac{P_{\text{simulation}} - P_{\text{acquired}}}{P_{\text{Rail}}} \times 100 \qquad \text{Eq. (12)}$$

It is clear by looking at Figure 13 that the model-based approach can predict pressure waves with high accuracy (error ±3%), as well as when the pressure oscillation varies significantly (ET 700 μs) from its typical behavior (ET 300/400/600 μs). Starting from the error definition (Equation 12) during the pressure wave propagation phase, to evaluate the pressure waves reconstruction accuracy for all tested conditions, the Root Mean Square Errors (RMSE) have been calculated. Figure 14 summarizes the pressure wave reconstruction in terms of RMSE with respect to ET and injection pressure. The

FIGURE 12 SI-PWR strategy using the MSD model-based approach.

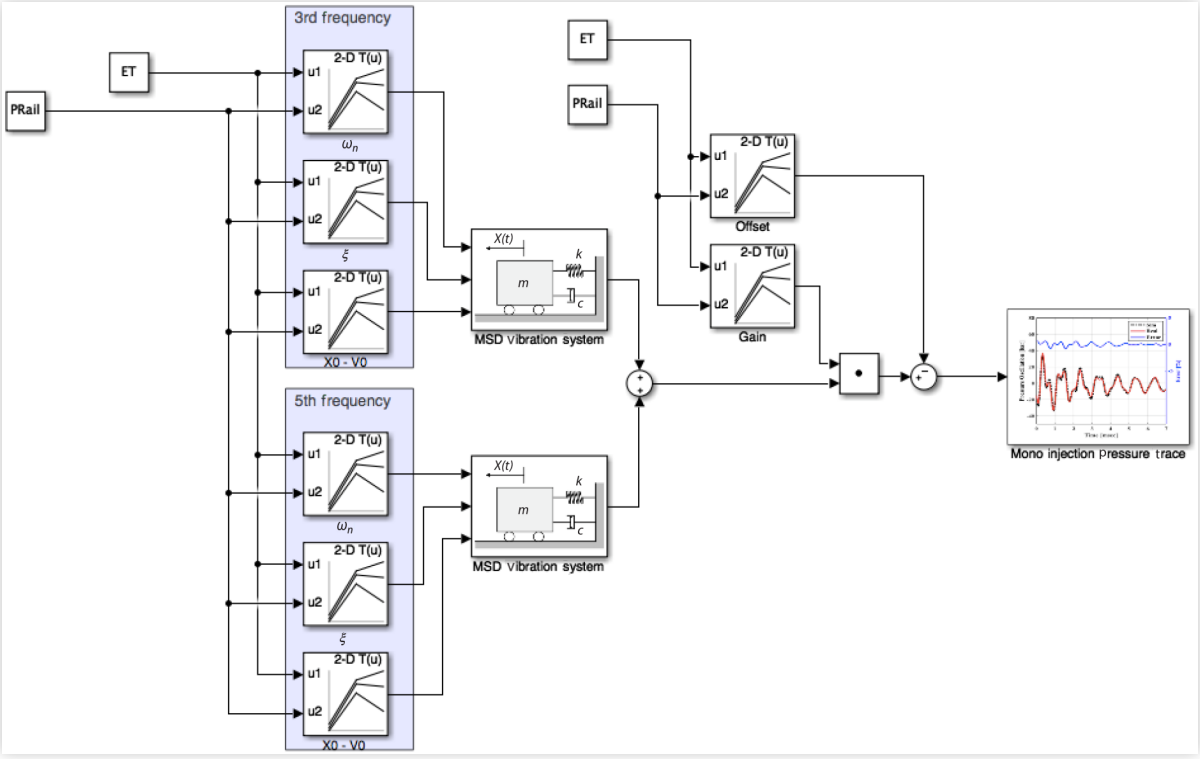

FIGURE 13 Comparison of experimental and reconstructed pressure waves and instantaneous error evaluation using the SI-PWR strategy with gasoline pressure of 700 bar, 1000 pump rpm, and ET of (a) 300 μs, (b) 400 μs, (c) 600 μs, and (d) 700 μs.

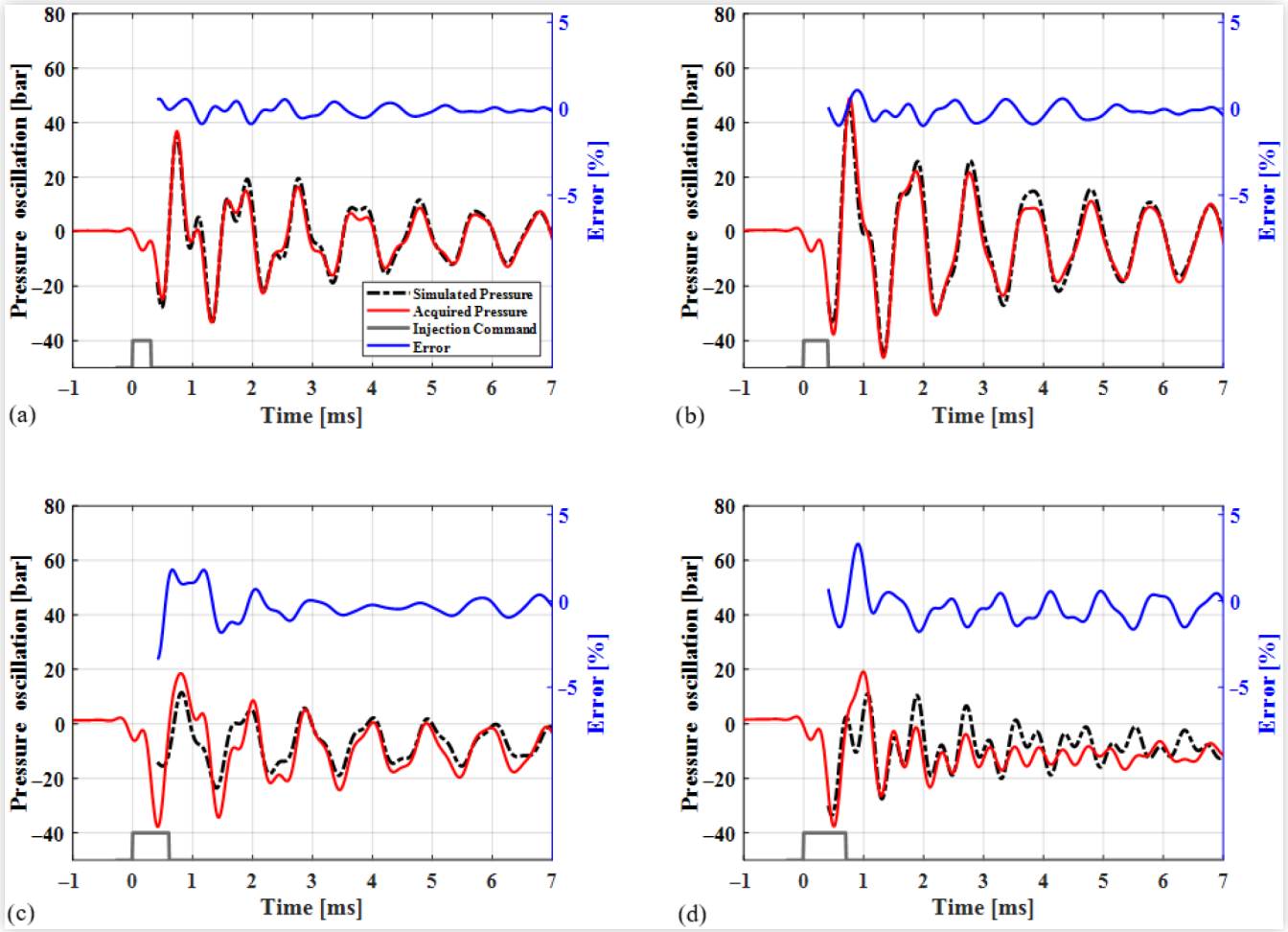

maximum RMSE of 1% reported in Figure 14 allows considering the model-based approach as valid for the SI-PWR.

To verify the information provided by the RCI in terms of the relevance of each carrier for the pressure wave reconstruction, the SI-PWR was tested in two different ways: only considering the fundamental frequency (simplified SI-PWR, with only the third main carrier) and adding the fifth carrier (SI-PWR). The results provided by the simplified SI-PWR were not sufficiently accurate (RMSE higher than 4%) especially for the tests operated at high ET [Figure 13(d)], where the contribution of the fifth frequency is clearly visible. As a result, the RMSE between the measured and the estimated instantaneous pressure drops to 1% considering, in the SI-PWR, also the fifth carrier. To further validate the information provided by the RCI, the model was tested also adding the second, the fourth, and both carriers, but this resulted in negligible improvements in the instantaneous pressure estimation. For this reason, the final SI-PWR approach has been designed considering only the third and fifth main carriers, as previously suggested by the RCI.

To check the model-based strategy robustness, the SI-PWR has been tested by changing fuel type and injectors. As widely reported in the literature [29, 34], the bulk modulus, defined in Equation 13, determines the hydraulic system's natural frequencies. Hence, changing fuel from gasoline to diesel, which is thicker than gasoline, at the same injection pressure and temperature will increase the hydraulic system's natural frequencies. Keeping constant the hydraulic system layout, the authors considered the fuel density variation effects on the system behavior as an offset, proportional to the square of the fuels density ratio [29], on the main frequencies values maps (ω_{n1} and ω_{n2}), as stated in Equation 14. Moreover, all the previously obtained hydraulic system parameters (ξ, x_0, and v_0) have been kept constant. Figure 15 shows the accuracy of the pressure waves reconstructions in terms of RMSE considering diesel fuel and placing the controlled injector in a different rail position, from position 3 to position 1 in Figure 2 [Figure 15(a)] or changing the activated injector (different hardware component but same injector type) with gasoline [Figure 15(b)]. Also, for these tested conditions, the low RMSE

FIGURE 14 Accuracy evaluation of the SI-PWR strategy (RMSE) using gasoline for all tested conditions of injection pressures and ET.

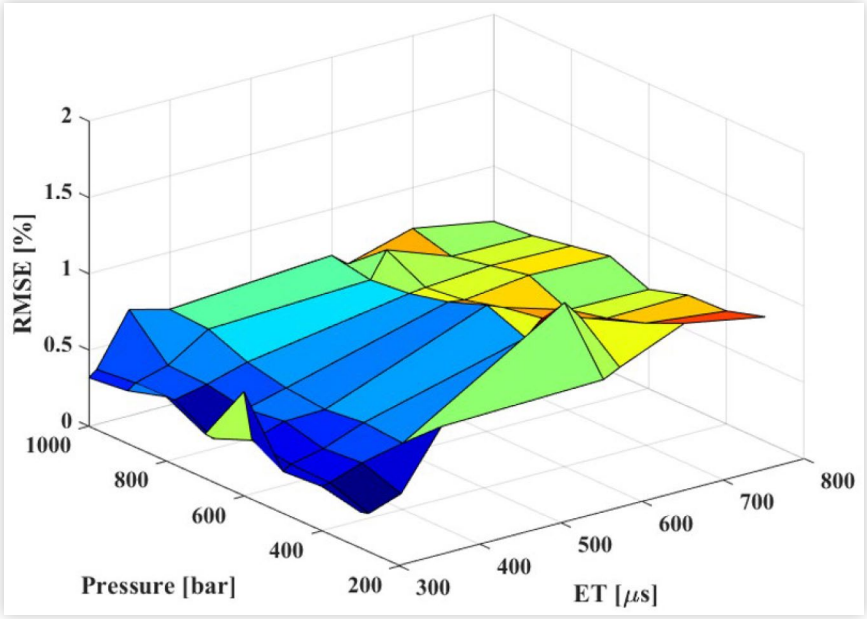

FIGURE 15 Accuracy evaluation of the SI-PWR strategy (RMSE) using the same injector fueled with diesel and different injector positions (a), and different injector (injector placement used for hydraulic system parameters calibration) fueled with gasoline (b) for all tested conditions of injection pressures and ET.

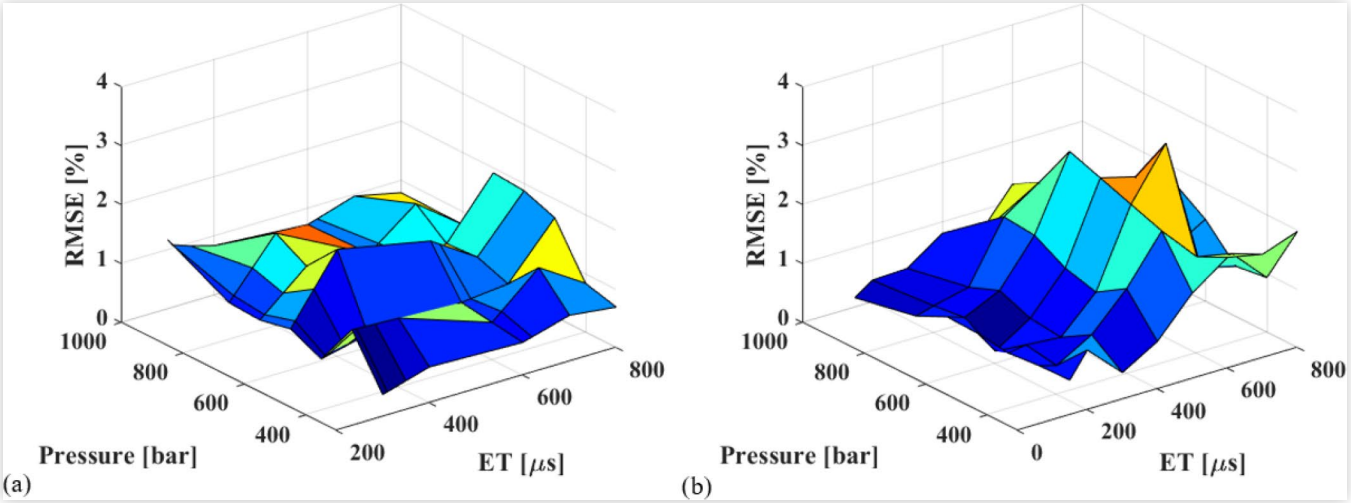

values underline the approach validity and robustness in the case of a single injection strategy.

$$K = \rho \frac{dP}{d\rho} \qquad \text{Eq. (13)}$$

$$\Delta_\omega = 1 - \sqrt{\frac{\rho_g}{\rho_d}} \cong 7\% \qquad \text{Eq. (14)}$$

It is important to notice that the model-based approach only considers the injection pressure effect on the hydraulic system parameters. By the bulk modulus (K) definition (Equation 13) results that also the fuel temperature can modify the system behavior (because it changes the fuel density). Despite the fact that the impact of the fuel temperature on density and bulk modulus cannot be neglected [34], the model-based strategy implicitly considers this effect thanks to the hydraulic system parameters (ω_n, ξ, x_0, and v_0) optimization for each injection pressure. With the purpose of characterizing the fuel temperature effect on density and bulk modulus, a hydraulic layout modification is needed, adding rail temperature sensors to those already installed before the HP pump.

Pressure Wave Reconstruction for Multiple Injection Strategy

As mentioned before, to properly manage gasoline PPC, a multiple injections pattern, typically composed of several pilot injections followed by the main injection, is needed [14, 15, 16, 17, 18]. The pressure oscillation triggered by the first injection pulse strongly modifies the injected quantity of the following injections [30, 31, 32, 33, 34], mainly because the second injection pulse occurs when the pressure wave cannot be neglected yet.

To define the impact of the pressure wave on the total amount of fuel injected with multiple injections, a wide experimental activity testing double injections strategy, summarized in Table 3, has been carried out. Figure 16 shows the measured injected mass, normalized with respect to the theoretical total injected mass (calculated using the injector map), at different injection pressures changing the DT, from 0 to 3500 µs, between two consecutive injection pulses (ET1 = ET2 for each injection pressure) using gasoline. As previously described, the higher the injection pressure the higher the pressure wave frequency; thus, the injected fuel mass oscillation will occur at smaller DT. Figure 16 also reports the hydraulic fusion region (DT < 600 µs): due to the slow injector dynamics, when the injected mass gets high, consecutive injections get very

FIGURE 16 Effects of injection pressure and DT on the effective injected fuel, normalized with respect to the total injected mass, generated by a double injection strategy (ET1 = ET2 ~ 1 mg/str) using gasoline.

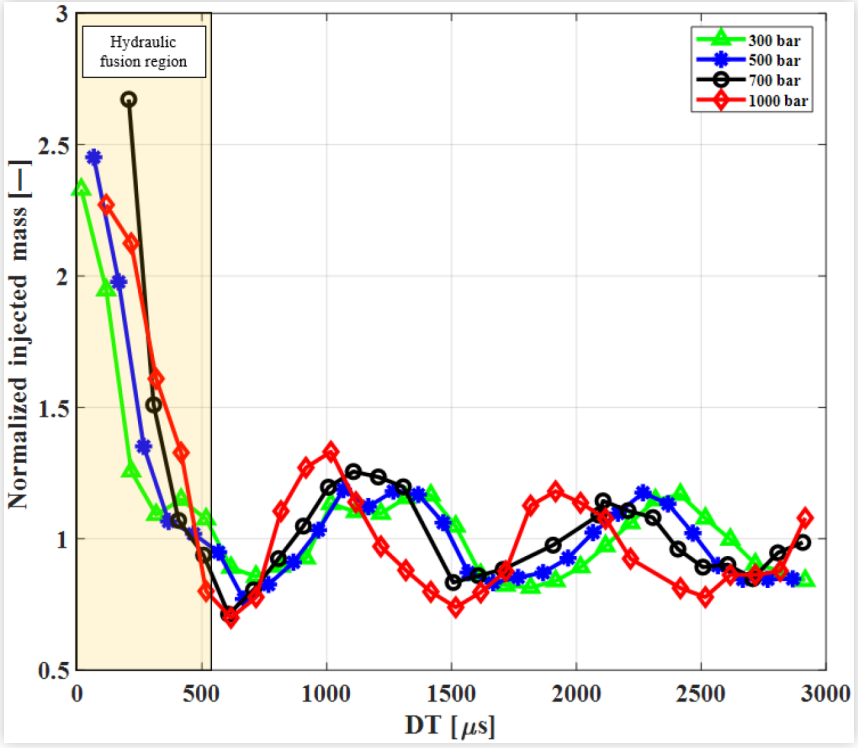

close [40, 42]. Considering the key role of the pilot injections on gasoline PPC management, the need of a compensation strategy for the injected fuel is mandatory to ensure the requested fuel mass on pilot injections (typical DT values for a multiple injection pattern are from 800 µs to 2500 µs).

To understand the behavior of the hydraulic system with a multiple injections strategy, the analysis of the pressure waves coming from the piezoresistive pressure sensors near the injector has been performed. Figure 17 shows the comparison of experimental pressure wave, triggered by single injection strategy, and the wave triggered by double injection strategy with the same ET. The reported pressure traces clearly highlight how the pressure wave generated by two consecutive injections can be considered as the sum of two single injection triggered pressure waves, shifted by DT. As a matter of fact, considering two consecutive injections with the same ET, the pressure wave generated by the first injection pulse does not modify either the amplitude or the frequency of the wave triggered by the following injection but only the fuel instantaneous pressure during the active phase of the injector (when the injector nozzle is open).

Based on the high accuracy of the SI-PWR applying the model-based approach, a pressure wave reconstruction for double injection strategy (DI-PWR) has been developed. Bearing in mind the previous considerations, the DI-PWR has been built as the sum of two SI-PWR. To simulate the pressure wave triggered by a double injection strategy, the scheme shown in Figure 18 has been used, in which the ET for both injections (ET1 and ET2), PRail and DT have been chosen as input variables. As it can be seen, the calculation structure replies twice (using the same hydraulic system parameters) the reconstruction strategy described in Figure 12.

Figure 19 shows the comparison of simulated and experimental double injection strategy pressure waves (considering only the oscillation contribution) for different DTs at a gasoline pressure of 700 bar and ET = 310 µs. It can be inferred from Figure 19 that both before and after the second injection pulse, the pressure wave has been simulated correctly. Moreover, it is possible to see that the reconstructions are consistent also during the active phase of the injector, providing reliable instantaneous pressure traces also with multiple injections strategies.

It is worth pointing out that as for the SI-PWR, the injector dynamics are neglected (especially during the injector closing); thus, the reconstruction accuracy decreases in the proximity of the injector closing. As mentioned before, this region (DT from 0 to 600 µs) should be avoided due to the hydraulic fusion; hence, this inaccuracy can be neglected. As made for SI-PWR, to summarize the simulations' accuracy, the RMSE for all tested DT and injection pressures have been calculated: results are reported in Figure 20. The maximum RMSE of 2% allows to consider the model-based approach as valid also for the DI-PWR. Based on the above-described

FIGURE 17 Comparison of experimental pressure wave triggered by double and single injection strategies at a gasoline pressure of 700 bar with the same ET = 310 µs, aligned with (a) first injection pulse and (b) second injection pulse.

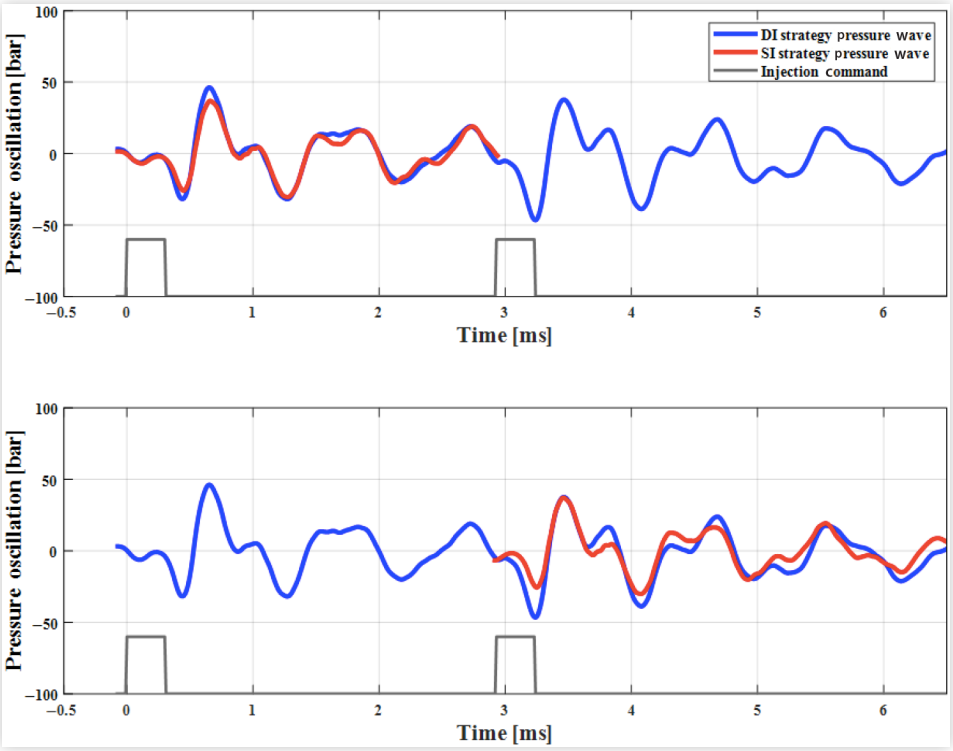

FIGURE 18 DI-PWR strategy based on the sum of 2 SI-PWR, using the MSD model-based approach.

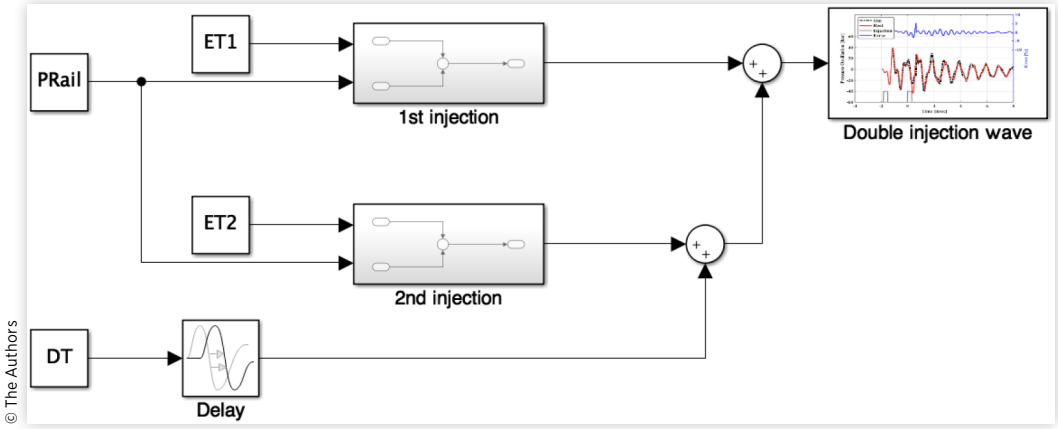

FIGURE 19 Comparison of the experimental and reconstructed pressure wave and instantaneous error evaluation using the DI-PWR strategy with a gasoline pressure of 700 bar, 1000 pump rpm, ET of 310 μs, and DT of (a) 1800 μs, (b) 2800 μs, (c) 3200 μs, and (d) 3900 μs.

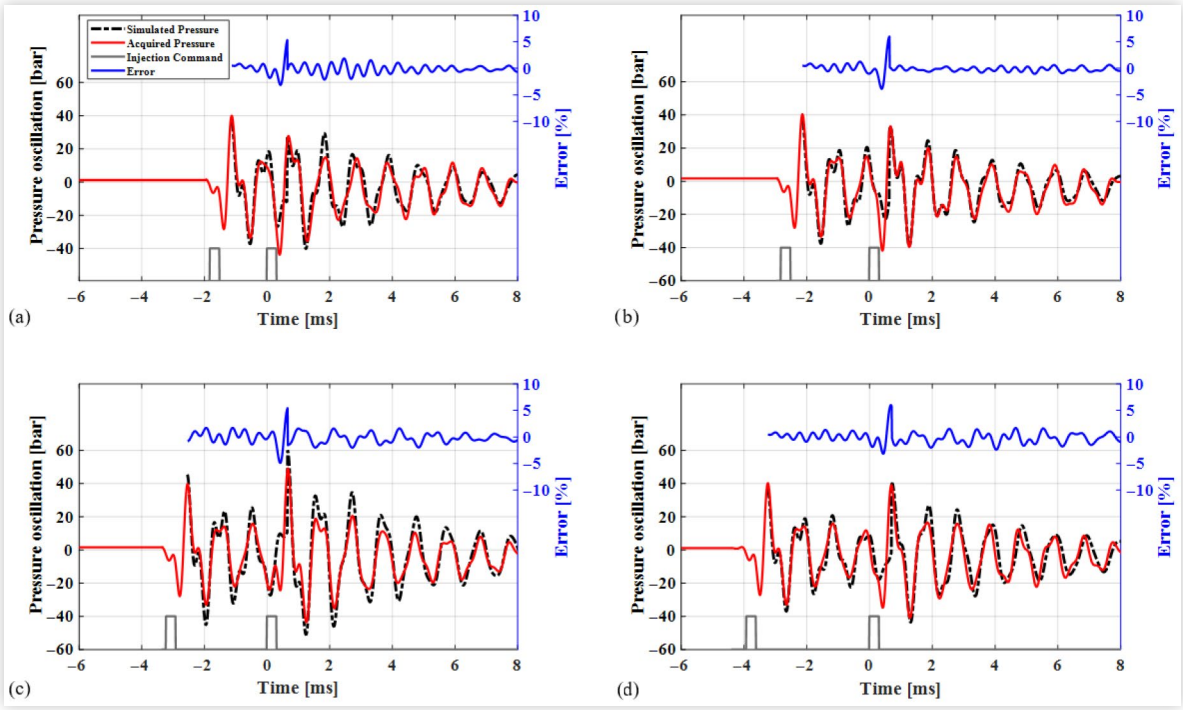

FIGURE 20 Accuracy evaluation of the DI-PWR strategy (RMSE) using gasoline (ET1 = ET2) for all tested conditions of injection pressures and DT.

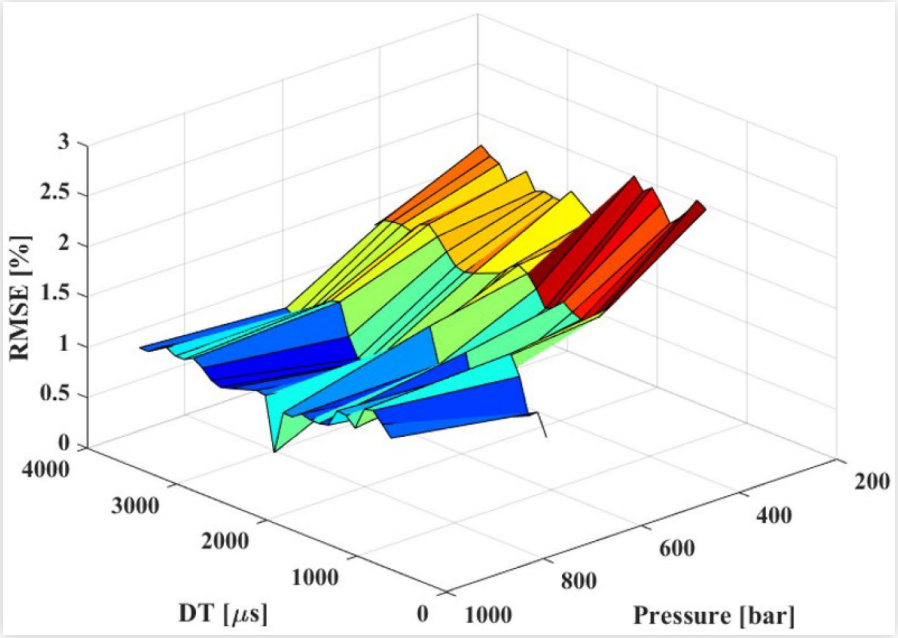

results referring to the modeling phase, the following section describes the fuel quantity FQC developed by the authors.

Fuel Quantity FQC

As explained in the previous section, the occurrence of pressure waves represents one of the most critical issues in CR systems for proper fuel injection management. The standard fuel dosing control strategies, both for single and multiple injections, are based on the rail-mounted pressure sensor, which does not contain the information of pressure oscillations. Especially for pilot injections, when the requested fuel mass is very low (m_{inj} ~ 1 mg/str) and DT < 2500 μs, the presence of the pressure oscillations modifies the second pulse injected mass, generating remarkable differences between the requested and effective total injected fuel [35, 36, 45]. Thus a fuel quantity FQC becomes crucial to manage gasoline PPC using a CR system, whereby the energy released by pilot injections plays a key role in ensuring the whole combustion process stability [14, 15, 16, 17, 46, 47, 48].

As a result of the high accuracy given by the DI-PWR, considering the effective pressure coming from the DI-PWR, a fuel-injected estimation was performed as the sum of the two injected masses (with ET1 = ET2) based on the injector map (without backpressure on the nozzle). Since the pressure wave does not affect the first injection, the injector map provides an accurate estimation of the amount of fuel introduced with the first injection using PRail (coming from the rail-mounted pressure sensor) and ET as inputs. With regard to the second injection, to compensate for the effects due to the pressure wave propagation triggered by the first one (injector closure), the estimation of the mass was carried replacing PRail with the average instantaneous pressure trace coming from the DI-PWR in the time interval corresponding to the activation of the second injection.

Figure 21 shows the comparison of measured and estimated (based on the DI-PWR) fuel consumption, normalized with respect to the total injected mass, for different DTs at a gasoline pressure of 1000 bar using gasoline. Despite the hydraulic fusion phase cannot be replied to by the DI-PWR, the estimated fuel consumption oscillations show good accordance with respect to the experimental both in terms of frequency and amplitude for each DT.

Based on the results obtained comparing the measured and estimated fuel consumption reported in Figure 21, with the aim of reducing the consumption oscillation during multiple injections, an FQC strategy has been designed, according to the block diagram reported in Figure 22. Relying on the instantaneous pressure wave reconstruction (applying the DI-PWR) during the second injection active phase, the FQC strategy can reasonably mitigate the fuel-injected quantity oscillations due to the effects of the pressure waves. As above described, the standard fuel dosing strategies are based on the rail-mounted pressure sensor, which does not contain the pressure oscillations; thus, with the aim of considering the pressure oscillations' effects on the second injection

FIGURE 21 Comparison of fuel quantity injected measured and estimated (with the DI-PWR considering the mean of the instantaneous pressure trace during the second injection active phase) during double injection strategy (ET1 = ET2) using gasoline at different DTs.

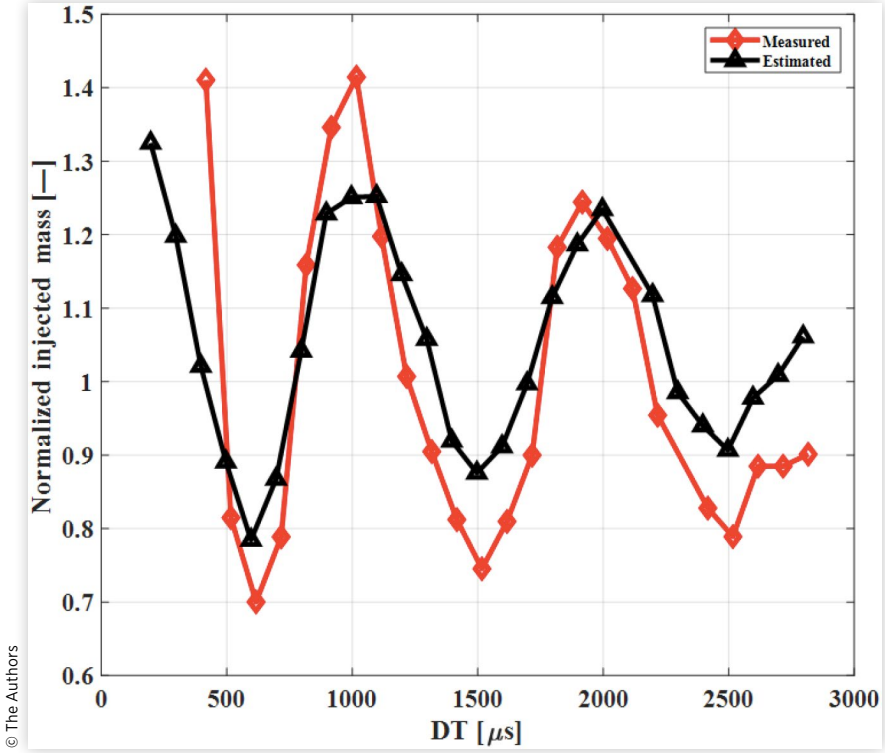

FIGURE 22 QFC strategy based on DI-PWR strategy using the MSD model-based approach.

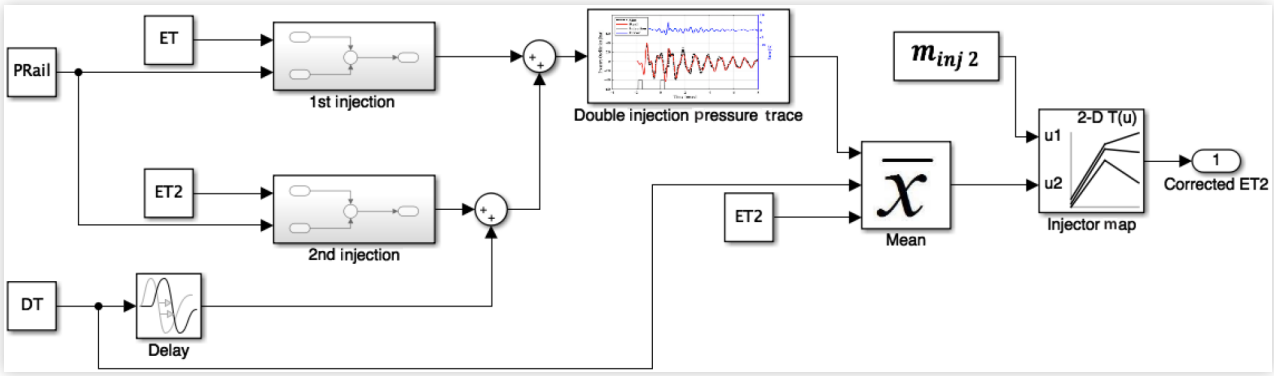

pulse, the rail-mounted pressure signal has been replaced by the DI-PWR. Since the pressure wave does not modify the first injected mass, the developed control strategy only modifies ET2, assuring the injected target mass $m_{inj\,2}$. It is important to notice that the FQC strategy is based only on previously defined 3D maps. Hence, after determining the hydraulic system parameter maps using the model-based approach, the FQC strategy can be easily implemented on a standard ECU.

Summary/Conclusions

This work presents a model-based pressure waves reconstruction strategy in a standard high-pressure CR system fueled with gasoline. To properly investigate pressure waves propagation in a CR system, a specifically developed flushing bench equipped with a high-frequency acquisition system has been realized, and to analyze the pressure waves in the CR system, the injector feed duct has been equipped with two additional high-pressure piezoresistive sensors.

A wide experimental activity has been carried out with different injection strategies, injection pressures, ET, and DT, aimed to evaluate the effects of the injection parameters on the hydraulic system behavior. By the analysis of the signals coming from the high-pressure sensors mounted on the flushing bench, it was possible to highlight the pressure waves behavior, and the modeling strategy was chosen based on the similarity with the free response of an underdamped MSD vibration system. To define the number of free responses able to properly reconstruct the pressure wave for a single injection strategy, a frequency analysis has been performed and the two main carriers have been identified for each tested condition. Finally, by using an optimization process based on MATLAB *fminsearch* function, both main carriers' MSD system parameters have been identified for each tested condition.

The MSD system parameters maps have been used to replicate the pressure wave generated by a single injection pulse strategy with different ETs and injection pressures. Despite the injector dynamics being neglected (the model accuracy slightly decreases after the nozzle closing), the SI-PWR performance evaluated both in terms of instantaneous pressure values and RMSE during the injection cycle proved the model-based approach accuracy for a single pulse injection strategy (RMSE < 1%) also when different fuel types and injectors were used (RMSE < 3%).

To compensate for the fuel quantity variation generated by very close and consecutive injections, several tests have been carried out to emphasize the impact of the second injection pulse on the pressure waves propagation. Experimental results clearly show that a pressure wave triggered by a double injection strategy (with ET1 = ET2) might be represented as the sum of two single injection pressure waves. Hence, based on the high accuracy given by the SI-PWR, the approach has been also applied to reproduce the pressure wave generated by a double injection strategy showing high accuracy (RMSE < 2%). Moreover, the comparison of measured and estimated fuel-injected quantities, based on averaging the reconstructed pressure trace during the second active injection phase, showed good accordance in terms of oscillation amplitude and frequency. Finally, using the model-based DI-PWR, to reduce the fuel quantity fluctuation especially for small injection pulses, an easily implementable FQC control strategy has been purposedly able to meet the very stringent requirement in terms of fuel dosing strategy performance running gasoline PPC.

Even though the presented approach proved to be robust and accurate (compatible with the requirements for its onboard application), further activity is currently being performed to update the experimental layout adding a temperature measurement in the feed duct of the injector, the goal is to evaluate the possible slight variation of the bulk modulus due to the fuel temperature variations.

Contact Information

Vittorio Ravaglioli
DIN—University of Bologna
vittorio.ravaglioli2@unibo.it

Definitions/Abbreviations

BEVs - Battery Electric Vehicles
BSFC - Brake-Specific Fuel Consumption
CDC - Conventional Diesel Combustion
CI - Compression Ignition
CR - Common Rail
DI-PWR - Double Injection Pressure Wave Reconstruction
DT - Dwell Time
ECU - Electronic Control Unit
EOI - End Of Injection
ET - Energizing Time
ET1 - First Injection Energizing Time
ET2 - Second Injection Energizing Time
FCEVs - Fuel Cell Electric Vehicles
FQC - Fuel Quantity Fluctuation Correction
HCCI - Homogeneous-Charge Compression Ignition
ICE - Internal Combustion Engine
K - Bulk Modulus
LTC - Low-Temperature Combustions
MSD - Mass-Spring-Damper
NOx - Nitrogen Oxides
PKist Inj Side - Piezoresistive fuel pressure sensor Injector Side
PKist Rail Side - Piezoresistive fuel pressure sensor Rail Side
PM - Particulate Matter
PRail - Rail Pressure

P_{r_x} - Relative power ratio of the *x*-th carrier
P_x - Amplitude of the *x*-th carrier
PWM - Pulse Width Modulation
RCI - Relevance Carrier Index
RCP - Rapid Control Prototyping
RMSE - Root Mean Square Error
RON - Research Octane Number
rpm - Revolutions per minute
SI-PWR - Single Injection Pressure Wave Reconstruction
SOI - Start of Injection
c - Fuel damping
dP - Pressure derivative
$d\rho$ - Density derivative
k - Fuel stiffness of the feed duct and injector
m - Fuel inertia
m_{inj} - Injected mass
$m_{inj\,1}$ - First pulse injected mass
$m_{inj\,2}$ - Second pulse injected mass
t - Time
x_0, v_0 - Initial Conditions
x_{01}, v_{01} - First main carrier estimated initial conditions
x_{02}, v_{02} - Second main carrier estimated initial conditions
Δ_ω - Natural frequency difference by different fuel type
ΔF_x - Frequency distance of the *x*-th carrier
$\sum_i P_i$ - Total energy of the identified main carriers
ξ_1 - First main carrier estimated damping ratio
ξ_2 - Second main carrier estimated damping ratio
ρ_d - Diesel density
ω_d - Damped frequency
ω_{n1} - First main carrier estimated natural frequency
ω_{n2} - Second main carrier estimated natural frequency

References

1. Bilgin, B. et al., "Making the Case for Electrified Transportation," *IEEE Transactions on Transportation Electrification* 1, no. 1 (2015): 4-17, https://doi.org/10.1109/TTE.2015.2437338.
2. Adnan, N., Nordin, S., Rahman, I., Vasant, P. et al., "An Overview of Electric Vehicle Technology: A Vision towards Sustainable Transportation," in IGI Global, *Intelligent Transportation and Planning* (Hershey, Pennsylvania, USA, 2018), https://doi.org/10.4018/978-1-5225-5210-9.ch013.
3. Emadi, A., *Advanced Electric Drive Vehicles* (Boca Raton, FL: CRC Press and Taylor & Francis Group, 2015)
4. Torregrosa, A.J., Broatch Jacobi, J.A., García Martínez, A., and Monico Muñoz, L.F., "Sensitivity of Combustion Noise and NOx and Soot Emissions to Pilot Injection in PCCI Diesel Engines," *Applied Energy* 104 (2013): 149-157, https://doi.org/10.1016/j.apenergy.2012.11.040.
5. Krishnamoorthi, M., Malayalamurthi, R., He, Z., and Kandasamy, S., "A Review on Low Temperature Combustion Engines: Performance, Combustion and Emission Characteristics," *Renewable and Sustainable Energy Reviews* 116 (2019): 109404, https://doi.org/10.1016/j.rser.2019.109404.
6. Dev, S., B Chaudhari, H., Gothekar, S., Juttu, S. et al., "Review on Advanced Low Temperature Combustion Approach for BS VI," SAE Technical Paper 2017-26-0042, 2017, https://doi.org/10.4271/2017-26-0042.
7. Dempsey, A.B., Curran, S.J., and Wagner, R.M., "A Perspective on the Range of Gasoline Compression Ignition Combustion Strategies for High Engine Efficiency and Low NOx and Soot Emissions: Effects of In-Cylinder Fuel Stratification," *International Journal of Engine Research* 17, no. 8 (2016): 897-917, https://doi.org/10.1177/1468087415621805.
8. Olsson, J., Tunestål, P., and Johansson, B., "Closed-Loop Control of an HCCI Engine," SAE Technical Paper 2001-01-1031, 2001, https://doi.org/10.4271/2001-01-1031.
9. Bengtsson, J., Strandh, P., Johansson, R., Tunestål, P. et al., "Control of Homogeneous Charge Compression Ignition (HCCI) Engine Dynamics," in *Proceedings of the 2004 American Control Conference, ACC*, Boston, MA, Vol. 5, 4048-4053, 2004, IEEE—Institute of Electrical and Electronics Engineers Inc., https://doi.org/10.1109/ACC.2004.182583.
10. Li, C., Yin, L., Shamun, S., Tuner, M. et al., "Transition from HCCI to PPC: The Sensitivity of Combustion Phasing to the Intake Temperature and the Injection Timing with and without EGR," SAE Technical Paper 2016-01-0767, 2016, https://doi.org/10.4271/2016-01-0767.
11. Dernotte, J., Dec, J., and Ji, C., "Investigation of the Sources of Combustion Noise in HCCI Engines," *SAE Int. J. Engines* 7, no. 2 (2014): 730-761, https://doi.org/10.4271/2014-01-1272.
12. Kolodziej, C., Dec, J., Lopez-Pintor, D., Pal, P. et al., "Advanced Compression Ignition Engines: Gasoline Range Fuels," in *2020 DOE Vehicle Technologies Office Annual Merit Review*, June 24, 2021, https://www.energy.gov/eere/vehicles/articles/advanced-compression-ignition-combustion-engines-gasoline-range-fuels.
13. Lahti, J. and Moskwa, J., "Dynamic Engine Control for HCCI Combustion," *SAE Int. J. Engines* 5, no. 3 (2014): 1133-1148, https://doi.org/10.4271/2012-01-1133.
14. Zhang, M., Xu, L., Derafshzan, S., Bai, X. et al., "Impact of Multiple Injection Strategies on Efficiency and Combustion Characteristics in an Optical PPC Engine," SAE Technical Paper 2020-01-1131, 2020, https://doi.org/10.4271/2020-01-1131.
15. Yin, L., Ingesson, G., Shamun, S., Tunestal, P. et al., "Sensitivity Analysis of Partially Premixed Combustion (PPC) for Control Purposes," SAE Technical Paper 2015-01-0884, 2015, https://doi.org/10.4271/2015-01-0884.
16. Dec, J., Dernotte, J., and Ji, C., "Increasing the Load Range, Load-to-Boost Ratio, and Efficiency of Low-Temperature Gasoline Combustion (LTGC) Engines," *SAE Int. J. Engines* 10, no. 3: 1256-1274, https://doi.org/10.4271/2017-01-0731.

17. Cho, K., Latimer, E., Lorey, M., Cleary, D. et al., "Gasoline Fuels Assessment for Delphi's Second-Generation Gasoline Direct-Injection Compression Ignition (GDCI) Multi-Cylinder Engine," *SAE Int. J. Engines* 10, no. 4: 1430-1442, https://doi.org/10.4271/2017-01-0743.
18. Stola, F., Ravaglioli, V., Silvagni, G., Ponti, F. et al., "Analysis of the Effects of Injection Pressure Variation in Gasoline Partially Premixed Combustion," SAE Technical Paper 2021-01-0517, 2021, https://doi.org/10.4271/2021-01-0517.
19. Stola, F., Ravaglioli, V., Silvagni, G., Ponti, F. et al., "Injection Pattern Investigation for Gasoline Partially Premixed Combustion Analysis," SAE Technical Paper 2019-24-0112, 2019, https://doi.org/10.4271/2019-24-0112.
20. Sellnau, M., Foster, M., Moore, W., Sinnamon, J. et al., "Pathway to 50% Brake Thermal Efficiency Using Gasoline Direct Injection Compression Ignition," SAE Technical Paper 2019-01-1154, 2019, https://doi.org/10.4271/2019-01-1154.
21. Sellnau, M., Cho, K., Zhang, Y., and Cleary, D., "Pathway to 50% Brake Thermal Efficiency Using Gasoline Direct Injection Compression Ignition (GDCI)," in *28th Aachen Colloquium Automobile and Engine Technology*, Aachen, Germany, 2019.
22. Nakai, E., Goto, T., Ezumi, K., Tsumura, Y. et al., "MAZDA SKYACTIV-X 2.0L Gasoline Engine," in *28th Aachen Colloquium Automobile and Engine Technology*, Aachen, Germany, 2019.
23. Buri, S., Kubach, H., and Spicher, U., "Effects of Increased Injection Pressures of up to 1000Bar—Opportunities in Stratified Operation in a Direct-Injection Spark-Ignition Engine," *International Journal of Engine Research* 11, no. 6 (2010): 473-484, https://doi.org/10.1243/14680874JER608.
24. Kimura, S., Aoki, O., Kitahara, Y., and Aiyoshizawa, E., "Ultra-Clean Combustion Technology Combining a Low-Temperature and Premixed Combustion Concept for Meeting Future Emission Standards," SAE Technical Paper 2001-01-0200, 2001, https://doi.org/10.4271/2001-01-0200.
25. Belgiorno, G., Dimitrakopoulos, N., Di Blasio, G., Beatrice, C. et al., "Parametric Analysis of the Effect of Pilot Quantity, Combustion Phasing and EGR on Efficiencies of a Gasoline PPC Light-Duty Engine," SAE Technical Paper 2017-24-0084, 2017, https://doi.org/10.4271/2017-24-0084.
26. Coppo, M., Dongiovanni, C., and Negri, C., "Numerical Analysis and Experimental Investigation of a Common Rail Type Diesel Injector," in in *ASME 2002 Internal Combustion Engine Division Fall Technical Conference*, New Orleans, LA, 271-280, 2002, https://doi.org/10.1115/ICEF2002-507.
27. Ubertini, S., "Injection Pressure Fluctuations Model Applied to a Multidimensional Code for Diesel Engines Simulation," *J. Eng. Gas Turbines Power* 128 (2006): 694-701, https://doi.org/10.1115/1.2135813.
28. Boundy, F. and Seers, P., "Impact of Physical Properties of Bio-Diesel on the Injection Process in a Common-Rail Direct Injection System," *Energy Conversion Management* 50 (2009): 2905-29102, https://doi.org/10.1016/j.enconman.2009.07.005.
29. Lee, J. and Lee, C.H., "An Uncertainty Analysis of the Time-Resolved Fuel Injection Pressure Wave Based on BOSCH Method for a Common Rail Diesel Injector with Varying Current Wave Pattern," *Journal of Mechanical Science and Technology* 32, no. 12 (2018): 5937-5945, https://doi.org/10.1007/s12206-018-1145-1.
30. Baratta, M., Catania, A.E., and Ferrari, A., "Hydraulic Circuit Design Rules to Remove the Dependence of the Injected Fuel Amount on Dwell Time in Multijet CR Systems," *Journal of Fluid Engineering* 130: 121104, https://doi.org/10.1115/1.2969443.
31. Bianchi, G.M., Falfari, S., Brusiani, F., Osbat, G. et al., "Numerical Investigation of Critical Issues in Multiple-Injection Strategy Operated by New C.R. Fast-Actuation Solenoid Injector," SAE Technical Paper 2005-01-1236, 2005, https://doi.org/10.4271/2005-01-1236.
32. Catania, A.E., Ferrari, A., and Manno, M., "Development and Application of Complete Common Rail Injection System Mathematical Model for Layout Hydro-Dynamic Analysis," in *ASME 2005 Internal Combustion Engine Division Spring Technical Conference*, Chicago, IL, 2005, https://doi.org/10.1115/ICES2005-1018.
33. Mohebbi, M., Azhar, A.A., Hamidi, A., Hajialimohammadi, A. et al., "Modeling of Pressure Line Behavior of Common Rail Diesel Engine due to Injection and Fuel Variation," *J. Braz. Soc. Mech. Sci. Eng.* 39 (2016): 661-669, https://doi.org/10.1007/s40430-016-0573-z.
34. Wu, D., Sun, B., Xu, A., An, X. et al., "Study on Pressure Fluctuation of a Constant Pressure Fuel System," SAE Technical Paper 2012-01-0828, 2012, https://doi.org/10.4271/2017-01-0828.
35. Ferrari, A. and Paolicelli, F., "Modal Analysis as a Design Tool for Dynamical Optimization of a Common Rail Fuel Injection System," SAE Technical Paper 2015-24-2467, 2015, https://doi.org/10.4271/2015-24-2467.
36. Catania, A., Ferrari, A., Manno, M., and Spessa, E., "Experimental Analysis of Transient Flow Phenomena in Multi-Jet Common Rail System," SAE Technical Paper 2005-24-048, 2005, https://doi.org/10.4271/2005-24-048.
37. Bai, Y., Gu, Y., Lan, Q., Fan, Y. et al., "Correction Strategy of Fuel Injection Quantity During Pilot-Main Injection of Common Rail System," *Journal of Mechanical Science and Technology* 34, no. 6 (2020): 2647-2656, https://doi.org/10.1007/s12206-020-0538-0.
38. Ferrari, A. and Paolicelli, F., (July 30, 2018), "Modal Analysis of Fuel Injection Systems and the Determination of a Transfer Function Between Rail Pressure and Injection Rate," *ASME. J. Eng. Gas Turbines Power.* 140, no. 11 (2018): 112808, https://doi.org/10.1115/1.403948.
39. Hai-feng, S., You-tong, Z., and Xu, L., "Damping the Water Hammer Pressure Wave in the High Pressure Common Rail System," *Transaction of CSICE* 31 (2013): 379-383.
40. Gupta, V.K., Zhang, Z., and Sun, Z., "Modeling and Control of Novel Pressure Regulation Mechanism for Common Rail Fuel Injection System," *Applied Mathematical Modelling* 35: 3473-3483, https://doi.org/10.1016/j.apm.2011.01.008.
41. Bianchi, G.M., Falfari, S., and Brusiani, F., "High-Pressure Wave Propagation Induced by Multiple-Injection Strategy Operated in a Common Rail Injection System Equipped by a Fast-Actuation Solenoid Injector," in *60th Congresso*

Nazionale ATI, Roma, September 13-15, 2005, Contributo in Atti di Convegno ART. 07/08.

42. Li, P., Zhang, Y., Li, T., and Xie, L., "Elimination of Fuel Pressure Fluctuation and Multi-Injection Fuel Mass Deviation of High Pressure Common Rail Fuel Injection System," *Chinese Journal of Mechanical Engineering* 28: 294-306, https://doi.org/10.3901/CJME.2014.1216.180.
43. Peng, J., Ma, M., Weizhi, W., Bai, F. et al., "Characterization of Rail Pressure Fluctuation under Two Injection Condition and the Control Strategy Based on ANN," SAE Technical Paper 2017-01-2212, 2017, https://doi.org/10.4271/2017-01-2212.
44. Kelly, S.G., *Mechanical Vibration Theory and Applications, SI* (Global Engineering, USA, 2012)
45. Heywood, J., *Internal Combustion Engine Fundamentals*, 2nd ed. (New York: McGraw Hill Education, 2018)
46. Bing-Qi, J., Li-Yun, F., Xiu-Zheng, M., Hayot, Q. et al., "Investigation of Main Injection Quantity Fluctuation due to Pilot Injection in a High Pressure Common Rail Fuel Injection System," *International Journal on Smart Sensing and Intelligent Systems* 7, no. 2 (2014): 820-836, https://doi.org/10.21307/ijssis-2017-683.
47. Ravaglioli, V., Ponti, F., and De Cesare, M., "Investigation of Gasoline Compression Ignition for Combustion Control," *J. Eng. Gas Turbines Power* 142, no. 9 (2020): 091003, https://doi.org/10.1115/1.4048055.
48. Matsuura, K. and Iida, N., "Effect of Temperature-Pressure Time History on Auto-Ignition Delay of Air-Fuel Mixture," SAE Technical Paper 2018-01-1799, 2018, https://doi.org/10.4271/2018-01-1799.
49. https://oilproducts.eni.com/en_GB/products/fuels/automotive, accessed October 2021.
50. Boehman, A.L., Morris, D., and Esen, E., "The Impact of the Bulk Modulus of Diesel Fuels on Fuel Injection Timing," *Energy & Fuels* 18, no. 6 (2004): 1877-1882, https://doi.org/10.1021/ef049880j.

Appendix A: Uncertainties

Further information about the additional sensors used by the authors to measure:

1. Fuel pressure: necessary to collect the information of the pressure waves

Sensor name	Kistler 4067A
Measuring range	0-2000 bar
Overload	500 bar
Sensitivity	5 mV/bar
Linearity	≤ ±0.5%
Natural frequency	>100 kHz

2. Fuel consumption: necessary to evaluate the total fuel injected mass

Sensor name	FlowSonic LF
Repeatability	±0.15% of reading
Uncertainty	±0.5% of reading
Measurement flow range	8-4000 ml/min
Measurement rate	2.2 kHz
Fluid temperature range	−20°C to +120°C
Ambient temperature range	−40°C to +120°C

3. Fuel consumption: necessary to evaluate the total fuel injected mass

Sensor name	AVL balance 733 s
Measuring range	0-150 kg/h
Uncertainty	±0.12%
Vessel capacity	1800 g

Appendix B: Fuel Specifications

Further information about the properties of the fuels used by the authors:

1. Automotive diesel properties [49]:

Fuel type	Unit	Automotive diesel
Density at 15°C	kg/m^3	820-845
Cetane number	—	51
Flash point	°C	55
Viscosity at 40°C	mm^2/s	2-4, 5
Biodiesel content	% (v/v)	0-7
Bulk modulus at 68.9 bar and 37.8°C [50]	GPa	1477

2. RON 95 gasoline properties [49]:

Fuel type	Unit	RON95
Density at 15°C	kg/m^3	720-775
RON	—	95
Flash point	°C	370
Viscosity at 50°C [50]	mm^2/s	0.45
Ethanol content	% (v/v)	0-5
Bulk modulus	GPa	N/A